This is a preprint, the final version is subject to change, of the American Mineralogist (MSA)
Cite as Authors (Year) Title. American Mineralogist, in press.
(DOI will not work until issue is live.) DOI: http://dx.doi.org/10.2138/am-2015-5008

Cation exchange capacity and water content of opal in sedimentary basins: example from the Monterey Formation, California

Revision 1

Arkadiusz Derkowski* [1], Jan Środoń [1], Douglas K. McCarty [2]

[1] Institute of Geological Sciences, Polish Academy of Sciences, Senacka 1, Kraków, 31-002 Poland.

[2] Chevron ETC, 3901 Briarpark Dr., Houston, TX 77042, USA

* Corresponding author, e-mail: ndderkow@cyf-kr.edu.pl

Abstract

Surface characteristics of sedimentary opal A and CT were investigated for a large collection of samples from the Monterey Formation, California, based on the bulk rock mineral and chemical analysis, cation exchange capacity (CEC) and water content. Two approaches were used: (1) modeling bulk CEC and adsorbed water content for the entire data set using the contents of opal and clay minerals measured by XRD, and (2), correcting the chemical composition and CEC of the most pure opal samples for the mineral impurities quantified by XRD.

Modeling indicates that the bulk rock data can be best explained by mixing an illite-smectite (CEC=59 meq/100g, 7-8% H_2O), consistent with the XRD characteristics of the clay fraction, with opal-A (8 meq/100g, 3.4% H_2O), or opal-CT (13 meq/100g, 3.7%H_2O).

Correcting the chemical composition of the most pure opal samples leaves a large excess of cations (Al, Fe, Na, K, Ca, and Mg). Iron is suspect to form traces of separate (oxy-)hydroxide

phases, not detected by XRD, while Al for Si substitution in the opal structure produced local negative charge, which was compensated by Na, K, Ca, and Mg exchange cations. A perfect balance of positive and negative charges is observed if the clay admixture in pure opals has the composition of montmorillonite. The concentration of heterogeneous impurities in silica network in opal leads to smectite formation on or within the diatom frustules. These dispersed smectite particles, perhaps monolayers, can be missed during the bulk rock mineral quantification.

The recalculated CEC of the opal, assuming the occurrence of dispersed smectite particles, varies from 3 to 11meq/100g, which is slightly less than that evaluated by modeling all the rock samples in the set, and corresponds to ~ 10-50% of the total opal charge quantified by the degree of Al for Si substitution. The remaining charge of the opal structure represents non-exchangeable cations. As opposed to smectite, opal CEC may depend on the size of cation used for the CEC measurement.

For opals in the Monterey Formation the content of water removable at 200ºC can be modeled as a sum of a constant value and a variable value dependent on CEC; the latter component is similar to the H_2O-CEC relationship that is typical for smectite. The combined system of a constant H_2O + variable H_2O in opal can potentially be applied for mineral modeling programs in wireline log formation evaluation in diatomaceous hydrocarbon reservoirs.

Keywords: opal, smectite, illite-smectite, cation exchange capacity, adsorbed water, Monterey Formation

INTRODUCTION

Cation exchange capacity (CEC) is among the most important physicochemical properties of sedimentary rocks. In the oil and gas industry, the CEC value reflects the quantity of hydrated cations, allows calculation of the mineral surface-bound water, and is used for various corrections and calibrations in wireline log analysis where it is employed in calculating effective porosity and permeability in hydrocarbon reservoirs (Clavier et al., 1984; Fertl and Chilingar, 1988; Brown and Ransom, 1996; Matteson et al., 2000). CEC is also important to hydrocarbon production, where it relates to formation damage potential, affects drilling and completion strategies, and is needed to design effective reservoir stimulation techniques.

One of the most common paradigms in measuring and modeling the sedimentary rock surface properties is the assumption that the bulk rock CEC and the total specific surface area (TSSA) are interrelated and control the quantity of adsorbed water *via* the content of hydrated cations, while CEC and TSSA of zeolite-free rocks are controlled almost exclusively by the quantity and type of clay minerals in a rock (Fertl and Chilingar, 1988; Kaufhold, 2006; Środoń and McCarty, 2008; Środoń, 2009; Środoń et al., 2009; Kaufhold et al., 2010). Therefore, the total adsorbed water in a sedimentary rock is essentially that of the clay-bound water (CBW). Clay minerals, including smectite, mixed-layered illite-smectite (I-S), and other, less common expandable mixed-layered clays (i.e. chlorite-smectite and kaolinite-smectite), contribute to the bulk CEC and TSSA, proportionally to their content in the rock, their expandability (%S; % of smectitic surfaces and interlayers), and the surface charge density (Q_s). Discrete illite has a CEC of about 15-20 meq/100g (Środoń et al., 2009) and is a minor contributor to the bulk CEC, while other micas and non-expandable clays, like chlorite and kaolinite, have negligible impact on the bulk CEC. In common diagenetic environments, such as sand-shale reservoirs, the typical range

of CEC values of the smectitic end-member of I-S is limited because of the narrow range of its layer charge density: $Q_s = 0.42 \pm 0.03$ (Środoń, 2009), which translates to the average CEC of ~110 meq/100g. Due to the narrow range of I-S surface charge densities and the fact that common pure smectite also has an average CEC value of 100meq/100g (Środoń and McCarty, 2008), the measured bulk CEC roughly represents the sum of smectitic surfaces in the sample. The CBW content is then directly calculated from the bulk, measured CEC (Clavier et al., 1984). In common sedimentary rocks, %S and weight percent of I-S and illite are the main factors determining bulk rock CEC and CBW. Rare sediments rich in zeolites do not follow this rule (Derkowski et al., 2006).

Opal derived from biogenic silica form a significant portion of mineral matrix in pelagic sediments, deposited in the upwelling zones. Because of the porous construction of the original diatom frustules, these deposits can have very high porosity and thus become exceptionally good hydrocarbon reservoirs (Montgomery and Morea, 2001; Cortese et al., 2004; Shukla and Mohan, 2012). After deposition, the silica occurs as opal-A (amorphous) and, with increasing diagenesis, it transforms into opal of a mixed crystoballite-tridymite layer structure (opal-CT) with progressively decreasing tridymite content, then into opal-C, which finally recrystallizes into quartz (Williams and Crerar, 1985; Guthrie et al., 1995; Elzea and Rice, 1996).

Natural opal as well as its synthetic analog was found to possess a variety of significant surface properties. Opal surface Si-OH groups provide a pH-dependent proton surface charge that varies among natural opal structures (Rodrigues et al., 2001; Khraisheh et al., 2005; Loucaides et al., 2010; Boboň et al., 2011; Ma et al., 2012). Aluminum dissolved in sea water complexes at the silica surface and can be incorporated into the silica structure (Gehlen et al., 2002; Koning et al., 2007; Houston et al., 2008). Substitution of Al and Fe for Si in the silica-silicate network is believed to produce local charge deficiency, which is compensated by the

93 exchangeable Na, Ca, K, Ba, and Mg cations (Beck et al., 2002; Gehlen et al., 2002; Gaillou et
94 al., 2008; Rondeau et al., 2012), as in phyllosilicates. The opal surface charge strongly increases
95 opal reactivity potential, raising a question of opal behavior during CEC measurements. For
96 example, Robertson and Twedily (1953) measured a very high CEC in pure diatoms, up to 54
97 meq/100g using exchange with ammonia, but only a fraction of this value was measured using
98 methylene blue. Moreover, a reaction of diatom frustules with saline water can result in
99 significant incorporation of a mixture of cations in the opal structure, which in turn can produce
100 authigenic smectite particles on or within diatom frustules (van Bennekom and van der Gaast,
101 1976; Badaut and Risacher, 1983; Michalopoulos et al., 2000; Gehlen et al., 2002).
102 Natural opals are known to contain large quantities of water, both in H_2O and OH forms,
103 up to 15 wt.%, in both opal A and opal CT structures (Jones and Renaut, 2004; Boboň et al.,
104 2011). The thermal release of the water species (dehydration and dehydroxylation) occurs at
105 different ranges of temperature with overlapping boundaries between them, but the majority is
106 usually released below 500°C (Graetsch et al., 1985; Mendioroz et al., 1989; Jones and Renaut,
107 2004). Webb and Finlayson (1987) linked different quantities of molecular H_2O and OH groups
108 to the Mg and Al substitutions in Si framework.
109 Regardless the actual origin and type of the opal surface charge, opal surface properties
110 and water content are expected to affect the petrophysical properties of the rock matrix in
111 diatomaceous sedimentary basins, and in particular the bulk rock CEC. The CEC/CBW ratio
112 could then be different than that known for clay minerals. The aim of this paper is to evaluate the
113 large-scale potential contribution of opals to the reservoir CEC and the adsorbed water content,
114 using a broad data set collected from the classic siliceous shale of the Monterey Formation in
115 California.
116

SAMPLES AND METHODS

Two types of samples have been used in the study:

1. *Mineral standards*. The standards represent several opal-A samples, a mixed-layer opal-CT, opal-C, and tridymite obtained from various sources, purified by chemical treatment and centrifugation. Structure and purity of the standards were checked by X-ray diffraction (XRD). Volcanic glass – obsidian, was used as a natural amorphous silica-rich reference to compare with the opal analysis.

2. *Natural samples from an opal-rich hydrocarbon reservoir*. Over 300 core samples were collected from numerous wells drilled by Chevron's San Joaquin Valley Business Unit in the Antelope shale of the Monterey Formation, San Joaquin Basin, California, USA (Montgomery and Morea, 2001). The samples represent an entire range of depths corresponding to the zones dominated by opal-A (~ 1000-1500 ft. in the study area) and the zones rich in opal-CT containing usually > 70% of cristobalite layers (~ 1300-1900 ft.) (Elzea and Rice, 1996; Chaika and Williams, 2001). The actual well names, locations, and sampling depths cannot be revealed due to industrial confidentiality.

Portions of mineral standards equilibrated at 50±3% relative humidity (RH) were analyzed for water loss at 110°C and 200°C (labeled H_2O110 and H_2O200, respectively) when held for 15 minutes at a given temperature, using the Mettler-Toledo HR83 moisture analyzer. According to Środoń and McCarty (2008) and Środoń et al. (2009), drying at 200°C is required to determine complete water loss from natural samples. The mineral standards were also analyzed for the continuous mass loss during heating by thermogravimetry (TG) using the TA 2050 analyzer connected to a mass spectrometer (MS) for evolved gas analysis. In the TG analysis ~

140 25 mg of a sample was heated from room temperature to 1000°C, with a rate of 5°C/min, under
141 N_2 gas flow of 25 ml/min.

142 All natural samples and mineral standards were analyzed for CEC using a broadly
143 applied, accurate, and fast spectroscopic method of CEC determination *via* exchange with
144 colorizing complex cations of high selectivity (Dohrmann, 2006 and references therein). In this
145 study CEC was determined using VIS spectrometry and Co(III)-hexamine chloride solution at
146 buffered pH ~ 7, following the method of Orsini and Remy (1976) and Bardon et al. (1993). A
147 pre-dried sample (0.5 – 1 g) was mixed with 25 ml of the Co(III)-hexamine stock solution at one
148 of the absolute concentrations of 14.95 mmol, 7.48 mmol, 3.74 mmol, and 1.5 mmol, shaken and
149 treated with ultrasounds for 2 minutes, then centrifuged for 10 minutes at ~ 4000 *g*. The
150 absorbance of the supernatant solution, analyzed at a wavelength of 470 nm linearly depends on
151 the amount of $[Co(NH_3)_6]^{3+}$cation, adsorbed by the tested sample.

152 Quantitative mineral analysis of bulk natural samples was performed using XRD analysis
153 on Thermo X'TRA diffractometer and the Quanta software (Chevron ETC proprietary), which
154 uses the mineral intensity factor method in conjunction with a collection of pure standards
155 (Środoń et al., 2001; Omotoso et al., 2006). The sample preparation procedure applied for the
156 samples was described by Środoń et al. (2001). The Quanta XRD standards contain a selection
157 of disordered and partially ordered structures of clay minerals and opal of various types and the
158 approach used has been proven successful in opal-rich and clay-rich samples (Omotoso et al.,
159 2006). In this method the total dioctahedral Al-rich 2:1 layer clay (illite, muscovite, dioctahedral
160 Al- and Al+Mg-smectite, mixed-layered illite-smectite) are quantified together by careful fitting
161 of the *060* reflection (Środoń et al., 2001) and are referred to as the illite+smectite group. The
162 structural details of the clay minerals that form this group are precisely identified and quantified

using the XRD patterns of oriented preparations of the < 2μm grain size fractions and the multi-specimen computer simulation method (e.g. Sakharov et al., 1999; McCarty et al., 2009).

Clay mineral composition was investigated in < 2μm grain size fractions, separated from selected natural samples after chemical purification and centrifugation including carbonate removal, organic matter (OM) oxidization, and Fe-(oxy-)hydroxides removal (Jackson, 1969). Diffraction data were collected from oriented preparations of the Ca-exchanged clay fractions in both the air-dry state and after saturation with ethylene glycol (EG). Qualitative and quantitative analyses were performed by full XRD pattern simulation using Sybilla software (Chevron proprietary, cf. McCarty et al., 2008), using the formalism described by Drits and Tchoubar (1990).

The chemical composition of the selected opal-rich, clay-poor samples (Table 1a) was analyzed with the common Inductively Coupled Plasma-Optical Emission Spectroscopy (ICP/OES), $LiBO_3$-fusion method, by Activation Laboratories Ltd., Ancaster, Ontario, Canada. Total organic carbon (TOC) was determined using a LECO elemental analyzer.

RESULTS

Bulk samples from the Monterey Formation

Natural samples were found to consist of four different mineral groups: (1) coarse detrital minerals (quartz > plagioclase > K-feldspar), (2) clay minerals (illite+smectite group >> kaolinite), (3) biogenic opals A and CT with minor opal-C, and (4) carbonate minerals either as cement (<10 wt.%) or as carbonate beds with higher carbonate contents. The samples represent a

range of opal content from zero to more than 90% (median 48%), and from zero to 27% of total clay minerals content (Figure 1 and 2) with a median of 12% for the illite+smectite group.

Due to potential variability of the opal and the I-S properties in the diagenetic zones of opal-A and opal-CT, the database of natural samples was divided into two roughly equal groups, based on the dominant opal type ("opal-A zone" and "opal-CT zone"). In these sample subsets the minor opal type is ≤ 5 wt.%.The CEC values measured in these zones vary from < 2 meq/100g to 17.3 meq/100g in the opal-A zone, and from < 2 meq/100g to 25.9 meq/100g in the opal-CT zone. H_2O200 values vary from 0.1 to 3.9 and to 4.1 wt.%, respectively (Figure 1 and 2).

The quantitative relationships between CEC or H_2O200 content and wt.% of the two components that can provide bulk rock CEC and H_2O200, i.e. opal and illite+smectite groups are similar for rocks with opal-A and opal-CT (Figures 1 and 2). There is no statistically significant linear correlation between neither CEC nor H_2O200 content and illite+smectite, but a very weak positive relationship can be observed between CEC and illite+smectite. The relationship between CEC and opal content has a clear, though scattered concave shape, while that for H_2O200 and opal content is linear, positive and less scattered, with a slight concave shape, especially for the opal-A samples.

The scattered, co-varying increase of illite+smectite mineral content with opal content up to ~30% (Opal A zone) and to ~ 50% (Opal CT zone) in the Figure 3 is responsible for an apparent control of CEC by opal at low opal contents (Figure 1 and 2). The illite+smectite *versus* opal relationships are, however, similar to the concave shapes of the CEC *versus* opal relationships (compare Figures 1 and 2 with Figure 3). Unless assuming that opal CEC is high in the samples with low opal content and it is much lower in the opal-rich samples, the similarity of these concave relationships suggests that illite+smectite content rather than opal is dominating

bulk CEC in the majority of the samples. The samples with intermediate opal content have the highest illite+smectite content and, therefore, the highest CEC. These relationships document that CEC and H_2O200 are controlled by different factors; CEC being more dominated by illite+smectite content while H_2O200 by opal content. The concave relationship of illite+smectite *versus* opal content is of sedimentary origin, because it characterizes both opal-A and opal CT samples, across the opal diagenetic transition.

A third subset of natural samples that contain at least 85% of opal-A and ≤ 5% of illite+smectite was selected from the database (11 opal-CT samples and 1 opal-A sample, Table 1). These samples can be considered as almost pure standards, where the measured bulk CEC and H_2O200 are negligibly affected by non-opal minerals. The opal-CT samples have CEC variability from 9.0 to 14.1 meq/100g (median 11.6 meq/100g) and H_2O200 values from 2.4 to 3.9% (median 3.3%). The opal-A sample has a CEC of 7.4 meq/100g and 2.4% of H_2O200. Due to difficulty in the quantification of disordered phases in amorphous matrix and the problem with determination of minerals with variable crystal chemistry, a careful quantification of minerals in the subset of the 12 opal-rich samples was repeated using various mineral standards, different than those used for the quantification of the majority of Monterey Formation samples. At low mineral contents, the relative quantification error is usually very high. The aim of the additional analysis was to find the highest acceptable content of minerals other than opal, in order to account for the chemical composition of the opal-rich samples. This procedure resulted in an increase in feldspar and carbonate contents by roughly 1% in respect to the previous quantification of the entire rock series, while illite+smectite content increased by 2-4 %, which is consistent with the assumed quantification errors. At such low concentrations the composition of the illite+smectite group cannot be determined in bulk samples. Only a discrete illite component was identified in some samples from sharp peaks close to 1 nm.

The composition of the<2 μm clay mineral fraction is similar in all samples, regardless the opal species. The samples have two types of mixed-layered illite-smectite, one with random interstratification (R0) and up to 19% of illite layers, and the other with ordered interstratification (R1) and 70-80% of illite layers. The discrete illite and kaolinite contents vary from 6 to 17 %, accompanied by a few percent chlorite (Figure 4).

Opal mineral standards

Three opal-A standards from different locations have CEC values from 3.5 to 6.0 meq/100g, in the following order: opal-A 586 > opal-A 282 >> opal-A 252. The lowest CEC among the opal-A samples is equal to that recorded for the opal-CT standard (3.6 meq/100g). Opal-C has 1.3 meq/100g, with is close to the CEC measurement limit, while the tridymite and obsidian samples have CEC values < 1 meq/100g (Table 2).

Water loss at 110°C and 200°C in the opal samples does not arrange samples in the same order as the CEC values. The opal-CT H_2O110 1.5% is close to the lowest value for the opal-A range (1.7 – 3.2%). There is a significant variability in the opal-A H_2O200 values, from 3.5 to 5.3%. In the opal-C, tridymite, and obsidian samples, the H_2O110 and H_2O200 values are low, ≤ 0.6 wt.%.

The TG patterns of the opal-A and CT standards have qualitatively similar features and can be divided into temperature ranges that correspond to different reactions. The first reaction seems to occur between room temperature and 300°C, and the second reaction is completed at about 650°C (Figure 5). Therefore, these two temperatures were chosen as reference values for

mass loss determination, TG-300 and TG-650, respectively, along with the final mass loss value at 1000°C, TG-1000 (Table 2).

The total TG mass loss of the opal-A and CT standards follow the order of mass loss determined for H_2O110 and H_2O200analysis with the moisture balance: opal-A 586 > opal-A 252 >> opal-A 282 > opal-CT 417 (Table 2). The final mass loss ranges for opal-A and CT are from 7.1 to 15.1 %. However, besides H_2O removal (mass 18), the evolved gas MS signal also showed the release of CO_2 (mass 44) in the temperature range of ~ 450-650°C. Therefore, the estimated range of maximum H_2O and OH loss in the opal-A and CT standards, derived from the TG-1000 values, has been reduced to 6 – 12 %, which is close to the loss of ignition (LOI) range measured for the opal-rich samples from the Monterey Formation (Table 1a), corrected for organic carbon (TOC) and the carbonate CO_2 content. The CO_2 evolved from the opal standards upon heating probably comes from organic matter as it is at lower temperature range than carbonate minerals, which were also not identified by XRD in the opal standards. The opal-C, tridymite, and obsidian standards have negligible mass loss during TG analysis, only< 0.5 wt.% at TG-650 and maximum 0.85wt.% at TG-1000, consistent with the mass loss determined with the moisture analyzer (Table 2).

MODELING THE OPAL CEC and H_2O200 IN SEDIMENTARY BASINS

The illite+smectite and opal phases are the main contributors to the CEC and H_2O200 in the sample set studied. Because illite+smectite CEC can be well constrained from the structural analysis (Środoń and McCarty, 2008; Środoń et al., 2009), it can serve as independent

verification for the modeling applied to estimate the corresponding CEC values for opal and illite+smectite.

The error minimization (F_{min}) approach, using the least-squares-based calculation was applied. It uses as the criterion of optimum solution the lowest difference between the bulk rock measured (CEC_{meas}, H_2O200_{meas}) and modeled (CEC_{model}, H_2O200_{model}) values for individual samples. The multi-variable linear regression model solving simultaneously multiple equations applied to the Monterey Formation sample set is:

$$F_{min} = \sum_n [(CEC_{meas} - CEC_{model})^2 + (H_2O200_{meas} - H_2O200_{model})^2] \quad \text{Equation 1}$$

and $$CEC_{model} = \frac{(CEC_{opal} \times W_{opal} + CEC_{I+S} \times W_{I+S})}{100} \quad \text{Equation 2a}$$

and $$H_2O200_{model} = \frac{(H_2O200_{opal} \times W_{opal} + H_2O200_{I+S} \times W_{I+S})}{100} \quad \text{Equation 2b}$$

where n is a number of samples (equations) solved simultaneously in a model; CEC_{opal}, H_2O200_{opal}, CEC_{I+S}, and H_2O200_{I+S} are the unknown values undergoing evaluation in this procedure, assumed in this calculation to be constant in the entire data set, while W_{opal} and W_{I+S} are known contents of opal and illite+smectite mineral group in a sample (in wt.%), respectively. The mineral quantification error can be as high as ±3 wt.% absolute for opals, due to their disordered structure, while it is up to ±2 % absolute for the illite+smectite mineral group (Omotoso et al., 2006). The CEC measurement error was considered as ±1 meq/100g (Derkowski and Bristow, 2012), while the repeatability of H_2O200 was determined to be ±0.1% with the moisture analyzer. For each sample, the CEC_{meas}, H_2O200_{meas}, W_{opal}, and W_{I+S} values were allowed to vary within these measurement error limits. The adjusted W_{opal} and W_{I+S} mineral contents, and the adjusted CEC_{meas} and H_2O200_{meas} values were thus fitted within the given maximum error to Equations 2a and 2b in order to minimize the F_{min} (Equation 1)

303 simultaneously, using the non-linear Solver® engine (Frontline Systems Co., Incline Village,
304 Nevada, USA).

305 The best fit between the measured and modeled bulk rock CEC values (Equation 1 and
306 2a), with the Pearson correlation coefficient $R^2 = 0.822$, was found in the opal-A zone for illite
307 CEC_{I+S} of 59.7 meq/100g and opal-A CEC value of 8.1 meq/100g. In the opal-CT zone the
308 highest correlation coefficient ($R^2 = 0.857$) was determined for CEC_{I+S} of 57.8 meq/100g and
309 opal-CT CEC value of 13.3 meq/100g (Figure 6). The calculated end-member H_2O200 values
310 (H_2O200_{opal}) that give the best fit between the measured and modeled bulk rock H_2O200 values
311 (Equation 1 and 2b) are 3.40 % for opal-A ($R^2 = 0.848$) and 3.68 % for opal-CT ($R^2 = 0.881$;
312 Figure 6). The calculated CEC_{opal} and H_2O200_{opal}values of both opals (A and CT) remain within
313 the ranges determined for almost pure opal samples from the Monterey Formation (Table 1b,c),
314 confirming validity of the model.

315 Careful simulation of the XRD patterns from the < 2μm clay fractions following the
316 approach by McCarty et al. (2008, 2009), revealed that the samples from both opal-A and opal-
317 CT zones contain a mixture of I-S phases, R0 and R1 in roughly equal proportions, regardless the
318 sample depth. This finding is different from the results by Compton (1991) who assigned the
319 occurrence of R1 ordering in I-S to opal-CT / quartz diagenetic transition, not seen in the opal-A
320 zone. Due to the independence of the degree of the opal diagenesis, here the I-S R0 and R1
321 phases are interpreted as being of detrital origin that have not underwent illitization. The
322 temperature of opal-A to opal-CT transition is broadly accepted as 35-50ºC, which is lower than
323 the onset of illitization (Keller and Isaacs, 1985; Compton, 1991; Huang et al., 1993). For the
324 Monterey Formation, an even lower temperature of 17 to 21 ºC was suggested for opal-A to opal-
325 CT transition (Matheney and Knauth, 1993).

The CEC of the total illite+smectite group (average for illite and different I-S populations) calculated from the composition of clay fractions varies within a narrow range of 53-67 meq/100g assuming an average 110 meq/100g for the smectite component in I-S and 15 meq/100g of CEC for the non-expandable illite layers (Figure 4). The CEC_{I+S} values calculated using Equation 2a are exactly within the CEC range for illite+smectite group found from the clay fractions, which provides independent evidence that the real CEC_{I+S} values cannot be significantly different than the calculated CEC_{I+S}. Therefore, to match the measured bulk rock CEC, the CEC of opal in the Monterey Formation samples also cannot be much different than the calculated CEC_{opal} values. Moreover, the CEC_{I+S} calculated independently for the opal-A zone and the opal-CT zone have essentially the same values with an insignificant difference, which provides additional validity for the models.

Additional confirmation of the modeling accuracy is that the modeled values for opal and illite+smectite explain the concave shape of CEC *versus* opal content curve (Figure 7). A simulation exercise was performed to verify the CEC *versus* opal content prediction model. The H_2O200 part was excluded from Equation 1. In two independent simulations the CEC_{opal} value in Equation 2a was fixed at zero or at 20 meq/100g, which is approximately twice the calculated CEC_{opal} value, and the simulations were performed again to find the lowest F_{min}. The third model with unconstrained CEC_{opal}, however, returned the CEC_{opal} and CEC_{I+S} values exactly the same as given by the models involving the H_2O200 part of the Equation 1 (Figure 6), reproducing perfectly the concave shape of CEC *versus* opal content. In both tested combinations with the constrained CEC_{opal}, the R^2correlation coefficient was significantly worse and the concave shape of CEC *versus* opal content was either not reproduced or followed with much lower quality of fit (Figure 7). For these two simulations, the calculated CEC_{I+S} values moved far beyond the range estimated from the clay fraction analysis, and corresponded to pure smectite when CEC_{opal} was

fixed at zero or to an almost pure illite when CEC_{opal} was set to 20 meq/100g (Figure 7). Therefore, the realistic range of CEC_{opal} values in the Monterey Formation must be much narrower than 0-20 meq/100g.

The calculated end-member H_2O200 values for the illite+smectite group (H_2O200_{I+S}) are 8.21 % in the opal-A zone and 6.71% in the opal-CT zone. Pure smectite equilibrated at 47% RH and heated at 200°C releases on average 16.0 wt.% of adsorbed water when Ca-exchanged and ~ 11.3 % when Na-exchanged (Środoń and McCarty, 2008); the same measurement conditions were applied for H_2O200 measurement in this study. The composition of exchangeable cations in the Monterey samples is unknown, but can be assumed to be a mixture of Na and Ca. Because the separated clay fraction has an ~50% equivalent smectite layer content in the total illite + illite-smectite (R1 and R0) minerals, the modeled H_2O200_{I+S} values (6.7-8.2 wt.%) match perfectly the values measured by Środoń and McCarty (2008).

DISCUSSION

Surface charge in biogenic opals from the Monterey Formation

Comparing the chemical and mineral composition of the twelve opal-rich samples provides an independent approach to evaluating the composition and surface properties of the opal species. Even if the maximum realistic non-opal mineral contents are used, the chemical composition does not match the mineral composition of the opal-rich samples (Table 1) if the opal fraction quantified by XRD is considered as pure SiO_2+H_2O.

Two chemical models were considered; assuming that the illite+smectite mineral quantified in the opal standards has a pure montmorillonite composition (average value from Środoń and McCarty, 2008), or it is the I-S with ~50%S, as estimated from the detailed clay analysis (Figure 4) and the CEC_{I+S} model (Figure 6). The I-S with ~50%S and a pure montomorillonite have different average chemical compositions, so they in turn contribute differently to the bulk rock element concentrations. For both applied models, after subtracting the contributions of all identified and quantified mineral species other than opal to the total element concentrations in the bulk rock, the excess K, Na, Al, Fe, Ca and Mg are observed in almost all samples analyzed (only Fe for one sample is slightly underestimated, Table 1b,c). The excess Al reaches up to > 1.0% while the average excess Na exceeds 0.3%. Assuming the negligible contribution from closed pore fluids, the excess element concentrations represent impurities in the opal silica network. If this model is correct, Al substitutes for Si and provides the negative net charge of silica while Na^{+}, Ca^{2+}, Mg^{2+} and K^{+} are then the compensating cations (Webb and Finlayson, 1987; Gehlen et al., 2002; Gaillou et al., 2008;). The valence of Fe in the studied samples is unknown. It is accepted that Fe^{3+}can behave like Al and substitute for Si (Rondeau et al., 2012). Alternatively, Fe may occur as separate, amorphous, XRD-undetectable oxy-hydroxide phase or linked to organic matter (van Bennekom and van der Gaast, 1976). Charge balance in the opal structure can be compared by assuming that the excess $(AlO_2)^{-}$ and $(Fe^{3+}O_2)^{-}$ are the species providing the negative charge excess in the silica network, and the monovalent and divalent cations compensate this negative charge (Table 1b,c, Figure 8). The charge balance tested with two different element excess sets of anions (from sole Al or total Al + Fe^{3+}) and the total cations, determined from two different illite+smectite mineral models (montmorillonite or I-S) shows a close qualitative match (Figure 8), which supports the model used. Despite good linear correlation, the models assuming total Al and Fe^{3+} substitution in the

397 silica framework have a significant deviation from the zero charge balance, with a trend line
398 slope << 1 for both mineral models. When assuming only Al substitution for Si (Gehlen et al.,
399 2002; Koning et al., 2007; Gaillou et al., 2008), the charge balance fit becomes perfect 1:1 for the
400 montmorillonite model, while the I-S model trend line displays a noticeable intercept of excess
401 positive charge (Figure 8). The calculation, therefore, suggests that Fe occurs outside the opal
402 structure as suggested by van Bennekom and van der Gaast (1976), the minor quantities of
403 illite+smectite mineral is represented mostly by smectite, and the silica network contains
404 abundant Al substitutions compensated by common seawater cations: Na, Ca, Mg, and K.
405 The bulk CEC measured for the opal-rich samples (Table 1a) can be reduced by the CEC
406 of re-quantified, maximum possible illite+smectite content, using either the I-S model (~60
407 meq/100g) or the montmorillonite model (100 meq/100g), in the same manner as calculating the
408 excess element concentrations. These "excess CEC" values, when normalized to the opal
409 content, represent the estimated CEC of pure opal, which - assuming the illite+smectite mineral
410 admixture as smectite - vary within 3-10 meq/100g (Table 1c). These values are consistent with
411 CEC measured for the pure opal standards (Table 2). The CEC_{opal} values modeled for opal-A and
412 opal-CT using the entire set of ~ 300 samples from the Monterey Formation (Figure 6) need to be
413 decreased by the CEC equivalent of 2-4 wt.% of smectite that the selected opal-rich samples
414 revealed after careful re-analysis (Table 1a). This brings the modeled CEC_{opal} values down to the
415 range of 4-11 meq/100g, as in the opal CEC range computed for the set of the twelve opal-richest
416 samples (Table 1c).
417 The CEC of the pure virtual opal accounts for only ~ 10-50% of the total opal charge
418 determined from Al substitution for Si (compare Table 1b,c). The mismatch between the CEC
419 and the total opal charge can be explained by distinguishing between the external (exchangeable)
420 and internal (fixed) compensating cations (*c.f.* Robertson and Twedily, 1953; Flörke et al., 2012)

in a similar way as performed for OH groups and Si-substituting cations by Webb and Finlayson (1987) and Loucaides et al. (2010). The Co-hexamine^{3+} cation used to measure CEC in this study is a large complex cation that does not enter micropores with a sub-nanometer effective size dimension (Derkowski et al., 2006). If smaller cations were applied for the CEC determination, more total compensating cations should be exchanged in the silica structure, as showed by Robertson and Twedily (1953). Using ammonia method those authors found CEC of pure opal samples in the range of 31-54 meq/100g comparing to 8-12 meq/100g determined with a large methylene blue molecule. The range of CEC determined with a large Co-hexamine cation and the total CEC estimated from excess ion based on chemical composition (Table 1c; Figure 8) perfectly match the ranges given by Robertson and Twedily (1953).

Opal chemical composition and smectite authigenesis

Smectite rather than detrital I-S particles embedded in the Monterey Formation opal structure should not be surprising. Van Bennekom and van der Gaast (1976), Badaut and Risacher (1983), Michalopoulos et al. (2000), and Gehlen et al. (2002) independently suggested the formation of very fine phyllosilicates within diatom particles. Most likely, such embedded smectite occurs mostly as monolayers, which is evidenced in the Monterey Formation opal-rich samples by the presence of the XRD *hk0* reflections that are proportionally much stronger than the corresponding *00l* reflections.

The presence of fine smectite crystallites (or even monolayers) associated with opal, in a combination with abundant Al substitutions in a silicate structure, suggests a specific pathway of smectite authigenesis in opals. The 1:1 charge ratio of total excess cations and Al implies the initial incorporation of tetrahedral Al into the silica network at an opal surface, rather than direct

nucleation of smectite precursor at a solid-water interface that would have to lead to a significantly lower cation/Al ratio and the presence of octahedral Al. Although a formation of Al^{IV}-rich, highly anionic aluminosilicate gel at opal surface seems a feasible mechanism (Robertson and Twedily, 1953; Michalopoulos et al., 2000; Houston et al., 2008), tetrahedral Al can also be incorporated directly into a diatom surface structure (Stoffyn, 1979; Gehlen et al., 2002; Flörke et al., 2012). A mix of Al^{IV} and Al^{VI} found in natural diatoms (Gehlen et al., 2002) also supports the idea that above a certain concentration of heterogeneous cations incorporated in opal structure smectite layers can form. The authigenesis of smectite particles from such an heterogeneous cation composition in the opal structure can be facilitated by the opal dissolution-precipitation during the opal-A→CT transformation (Compton, 1991; Williams and Crerar, 1995).

Water release from biogenic opals

Using the same approach as for the opal-normalized excess CEC calculation (Table 1b,c), H_2O200 measured for the opal-rich samples (Table 1a) can be reduced by the theoretical water adsorbed on associated clay, using either the I-S model (H_2O200 = 7 wt.%) or the montmorillonite model (H_2O200 = 14 wt.%), assuming mixed Na and Ca cations in the interlayer (Środoń and McCarty, 2008). The "excess H_2O200" values were then normalized to the opal content. These calculated H_2O200 values for pure opal from the Monterey Formation samples range from 2 to 4 wt.% (Table 1b,c), which is close to the H_2O200 values measured for the opal standards (3.5 - 5.3 wt.%; Table 2).

Plotting the computed excess (opal) H_2O200 *versus* excess (opal) CEC (Table 1b,c) reveals a weak positive correlation for the opal-rich Monterey samples, regardless the detailed

clay type assumed for the illite+smectite phase (Figure 9). Moreover, both the modeled opal-A and opal-CT, CEC_{opal} and H_2O200_{opal} values (Figure 6), reduced by ~3% contribution of virtual smectite, occur close to the trend line derived from the opal-rich Monterey samples. Although the actual opal H_2O200/CEC ratio determined for these samples varies significantly from 0.3 to 1.0, a linear equation with an intercept of ~ 1.75 wt.% of H_2O200 for zero-CEC describes the opal H_2O200 and opal CEC relationship with an average factor of 0.17 (SD = 0.066; Figure 9). The very same H_2O200/CEC ratio has been measured for pure smectite (Środoń and McCarty, 2008; Kaufhold et al., 2010). Although these two values may be coincidental, they can as well suggest that a portion of the water removable from opal A and CT at 200ºC is controlled by the hydration of exchangeable cations like in expandable clays, and that content of such water varies among samples from the same formation. Alternatively, the linear correlation between CEC and H_2O200 can be provided by anhydrous, amorphous, Al-rich, gel-like aluminosilicate phase formed at opal surfaces (Robertson and Twedily, 1953; Michalopoulos et al., 2000; Houston et al., 2008). In contrast, the other portion of adsorbed water in opal, described by the intercept, is cation-independent and it is relatively constant for the entire sample set. This fraction of water likely represents H_2O bound directly to Si-OH surface groups (Loucaides et al., 2010; Boboň et al., 2011). Two opal standards strongly deviate from the general trend of the H_2O200 *versus* CEC in the Monterey Formation samples (Figure 9). Such variability is not uncommon because opal surface properties can vary significantly (Van Cappellen, 1996; Rodrigues et al., 1999; Boboň et al., 2011).

Because residual H_2O molecules are still noticeable in opal after drying in a vacuum at 200°C (Boboň et al., 2011), the observed transition on the TG curve between the low-temperature and the high-temperature mass loss at ~300°C (Figure 5) can be assigned to the complete removal of water molecules and the beginning of breaking O-H bonds in silanol groups. Further

493 continuous mass loss, besides organic matter decomposition, is thus interpreted as subsequent
494 dehydroxylation of silanol groups, forming H_2O molecules, starting from the opal surface and
495 proceeding deeper into the opal structure. Water and OH groups may also be released from fluids
496 contained in closed porosity (Khraisheh et al., 2005; Boboň et al., 2011).

497 As found in this study and by other authors, H_2O and OH contents vary significantly in
498 opal-A and opal-CT structures (Jones and Renaut, 2004; Boboň et al., 2011). The structural
499 transition of opal-CT to opal-C and to chalcedony results, however, in an immediate loss of total
500 water content (Graetsch et al., 1985) and CEC (Table 2). The diagenetic reaction of opal-CT to
501 opal-C must release enormous quantities of water, thus strongly change the local geochemical
502 environment. Comparing the quantities of total water (H_2O + OH) potentially releasable from
503 opal (median content 48 % with 6-12% water) and illite+smectite mineral group (median content
504 12% with 11-13% water), it appears that the total liquid locked up by opal in the Monterey Fm.
505 rocks can be much greater than the total H_2O + OH in clay minerals. When released by frictional
506 heating during earthquakes, this expelled water can strongly affect the energetics and propagation
507 of earthquakes (Hirono and Tanikawa, 2011), which is especially significant in the neighboring
508 San Andreas Fault system in central California.
509

510 IMPLICATIONS OF OPAL SURFACE PROPERTIES FOR HYDROCARBON
511 EXPLORATION IN DIATOMACEOUS RESERVOIRS

512

513 Different fractions of water in the opal structure and opal surface properties affect wire-
514 log measurements and require a revision of conventional approach to porosity determination.
515 Not only the molecular weight divided by unit cell volume (in ordered structures) or atomic
516 weights and packing factor (in amorphous phases) are the controlling factors for mineral density,

517 but also the quantity of OH groups and their surface distribution strongly affects the mineral
518 density of opals A and CT (Chaika and Williams, 2001; Boboň et al., 2011). The opal water
519 would greatly mislead the wireline log-based neutron-porosity determination and may provide
520 significant mismatch between the density, nuclear magnetic resonance (NMR), and resistivity
521 logs when conventionally interpreted (Pearson and Derbyshire, 1974; Clavier et al., 1984;
522 LeCompte et al., 2008). The same tendency may occur when trying to calculate the CBW-
523 equivalent for opals; the dual-water theory models will not be valid for opal-A and CT in the
524 same way as it works for clay minerals (Clavier et al., 1984; Fertl and Chilingar, 1988; Matteson
525 et al., 2000). Due to a multi-step mass loss during opals heating, there is no clear boundary
526 between different fractions of H_2O and OH, therefore the notion of "dry mineral" in the case of
527 opal-A and CT may not have any practical meaning in oil exploration.
528 The relationship in Figure 9, gives hope for linking the conventional dual-water theory
529 model to the opal-bound water. A portion of the opal-bound water can be CEC-dependent in a
530 similar way as on the surfaces of clay minerals (Clavier et al., 1984; Kaufhold et al., 2010) while
531 the intercept of the linear function of adsorbed water *versus* CEC is probably a formation-specific
532 constant that can be determined by careful mineralogical studies and quantitative analysis. The
533 combined system of a constant H_2O in opal + variable H_2O, related to CEC as in smectite can
534 potentially be applied for mineral modeling programs in wireline log formation evaluation (Fertl
535 and Chilingar, 1988; Brown and Ransom, 1996; Zorski et al., 2011). Because two other opal
536 standards do not follow the trend line formed by the Monterey samples, it is clear that a separate
537 study is required for separate basins.
538 As opposed to smectite, opal CEC may depend on the size of cation used for the CEC
539 measurement in a similar manner as in zeolites (Robertson and Twedily, 1953; Derkowski et al.,
540 2006). Opal surface charge is pH-dependent with zero point charge at pH 5-6. At pH 10 opal

surface charge density can increase to 0.5-0.6 C/m^2, which is several times greater than smectite, while below pH 5 silica surface can develop anion exchange capacity (Rodrigues et al., 2001; Ma et al., 2012). Such variability of opal surface properties with pH, within the pH range common for pore water chemistry, affects the reservoir stimulation process (Montgomery and Morea, 2001). The adsorption of dyes as a function of pH was found, however, far less variable than the surface charge density (Khraisheh et al., 2005), so the opal surface adsorption properties under formation conditions may depend also on a type of adsorbate reagent used in a reservoir stimulation flow (*cf*. Robertson and Twedily, 1953). Therefore, the CEC value measured for opal at a given pH in the laboratory can serve as reference but the actual formation CEC likely varies with the pH and chemical composition of pore water. Moreover, silanol pH-dependent surface properties may produce an alteration in opal surface wettability, from water-wet to oil wet, decreasing the efficiency of recovery (Turov and Leboda, 1999; Strand et al., 2007).

CONCLUSIONS

Recent developments in routine mineral quantification of non- and semi-crystalline phases allowed combining quantitatively bulk rock CEC data and the adsorbed water content with clay minerals and opal contents. Opal A and CT are found to have measurable CEC. Opal CEC varies even within one formation due to the different degree of Al for Si substitution in the silica network structure, producing local negative charge that is compensated by potentially exchangeable Na, K, Ca, and Mg cations.

The range of CEC values found for opal-A and opal-CT in the Monterey Formation is 3-11 meq/100g, which is a fraction of the total charge determined by the Al substitution in the silica network. The other portion of total charge is not available for cation exchange by the applied

565 method. Opal CEC can be both exchange cation-dependent and pH-dependent, which is a topic
566 for future studies.

567 Dispersed smectite particles identified in the opal samples from the Monterey Formation
568 are easily underestimated or missed by routine XRD-based mineral quantification. The formation
569 of authigenic smectite particles within opals, or on opal frustule surfaces have been found in
570 various environments and can be much more common than assumed to date.

571 Although the absolute CEC of opal surface measured with Co-hexamine cation is quite
572 low, lower than a typical illite, the opal contribution to the bulk rock CEC can be significant due
573 to opal forming large proportions of the mineral matrix. Due to a great variability and number of
574 OH groups and attached water molecules on opal surface and trapped within closed pores, the
575 CEC-to-total opal water ratio does not follow the relationships determined for clay minerals. In
576 the Monterey Formation, the opal-bound adsorbed water removable at 200ºC, seems to develop
577 two components: (1) a constant quantity specific for the formation, and (2) a variable quantity
578 that is CEC-dependent, similar to the CBW/CEC relationship for clay minerals. Additional work
579 will help verify this concept.

580

581 **Acknowledgements**

582 Dale Julander and the Chevron Corporation San Joaquin Valley Business Unit team are
583 greatly acknowledged for providing the samples, financial support, and permission to publish the
584 results. We thank Bruce McCollom, Kymberli Correll, and Prince Ezebuiro from Chevron ETC
585 laboratories in Houston for essential laboratory work. Marta Labocha kindly helped with the
586 statistics. We are grateful to Marek Szczerba for his criticism. Helpful comments and
587 suggestions from the reviewer Panagiotis Michalopoulos and Warren Huff greatly improved the
588 paper.

589

590 **REFERENCES**

591

592 Badaut, D. and Risacher, F. (1983) Authigenic smectite on diatom frustules in Bolivian saline
593 lakes. Geochimica et Cosmochimica Acta, 47, 363-375.
594 Bardon, C., Bieber, M.T, Cuiec, L., Jacquin, C., Courbot, A., Deneuville, G., Simon, J.M.,
595 Voirin, J.M., Espy, M., Nectoux, A., and Pellerin, A. (1993) Recommandations pour la
596 determination experérimentale de la capacité d'échange de cations des milieux argileux.
597 Revue de l' Institut Francais du Pétrole, 38, 621-626.
598 Beck, L., Gehlen, M., Flank, A.-M., Van Bennekom, A.J., and Van Beusekom, J. E. E. (2002)
599 The relationship between Al and Si in biogenic silica as determined by PIXE and XAS.
600 Nuclear Instruments and Methods in Physics Research B, 189, 180–184
601 Boboň, M., Christy, A.A., Kluvanec, D., and Illášová L. (2011) State of water molecules and
602 silanol groups in opal minerals: a near infrared spectroscopic study of opals from
603 Slovakia. Phys Chem Minerals, 38, 809–818.
604 Brown, K.M. and Ransom, B. (1996) Porosity corrections for smectite-rich sediments: Impact on
605 studies of compaction, fluid generation, and tectonic history. Geology; 24, 843–846.
606 Chaika, C. and Williams, L.A. (2001) Density and mineralogy variations as a function of porosity
607 in Miocene Monterey Formation oil and gas reservoirs in California. AAPG Bulletin, 85,
608 149–167.
609 Clavier, C., Coates, G., and Dumanoir, J. (1984) Theoretical and Experimental Bases for the
610 Dual-Water Model for Interpretation of Shaly Sands. Society of Petroleum Engineers
611 Journal, 24, 153 – 168.

612 Compton, J.S. (1991) Origin and diagenesis of clay minerals in the Monterey Formation, Santa
613 Maria Basin area, California. Clays and Clay Minerals, 39, 449-466.
614 Cortese, G., Gersonde, R., Hillenbrand, C.-D., and Kuhn, G. (2004) Opal sedimentation shifts in
615 the World Ocean over the last 15 Myr. Earth and Planetary Science Letters, 224, 509–
616 527.
617 Derkowski, A. and Bristow, T.F. (2012) On the problems of total specific surface area and cation
618 exchange capacity measurements in organic-rich sedimentary rocks. Clays and Clay
619 Minerals, 60, 348–362.
620 Derkowski A., Franus W., Beran E., and Czímerová A. (2006) Properties and potential
621 applications of zeolitic materials produced from fly ash using simple method of synthesis.
622 Powder Technology, 166, 47-54.
623 Drits, V.A. and Tchoubar, C. (1990) X-ray Diffraction by Disordered lamellar Structures, p. 371.
624 Springer-Verlag, Berlin.
625 Dohrmann, R. (2006) Cation exchange capacity methodology II: A modified silver–thiourea
626 method. Applied Clay Science, 3, 38–46.
627 Elzea, J.M. and Rice, S.B. (1996) TEM and X-ray diffraction evidence for cristobalite and
628 tridymite stacking sequences in opal. Clays and Clay Minerals, 44, 492-500.
629 Fertl, W.H. and Chilingar, G.V. (1988) Determination of Volume, Type, and Distribution Modes
630 of Clay Minerals from Well logging Data. Society of Petroleum Engineers Journal,
631 SPE17145, 13-28.
632 Flörke, O.W. and 15 co-authors (2012) Silica. In: Ullmann's Encyclopedia of Industrial
633 Chemistry, 7th Edition (Ed. Bellussi, G. et al.), Wiley-VCH Verlag GmbH & Co. KGaA,
634 Weinheim, pp. 421-507.

635 Gaillou, E., Delaunay, A., Rondeau, B., Bouhnik-le-Coz, M., Fritsch, E., Cornen, G., and
636 Monnier, Ch. (2008) The geochemistry of gem opals as evidence of their origin. Ore
637 Geology Reviews, 34, 113-126.
638 Gehlen, M., Beck, L., Calas, G., Flank, A.-M., Van Bennekom, A.J., and Van Beusekom, J. E. E.
639 (2002) Unraveling the atomic structure of biogenic silica: Evidence of the structural
640 association of Al and Si in diatom frustules. Geochimica et Cosmochimica Acta, 66,
641 1601–1609.
642 Graetsch, H., Flörke, O.W., and Miehe, G. (1985) The Nature of Water in Chalcedony and Opal-
643 C from Brazilian Agate Geodes. Phys. Chem. Minerals, 12, 300-306.
644 Guthrie, G.D., Jr., Bish, D.L., and Reynolds, R.C., Jr. (1995) Modeling the X-ray diffraction
645 pattern of opal-CT. American Mineralogist, 80, 869-872.
646 Hirono, T. and Tanikawa, W. (2011) Implications of the thermal properties and kinetic
647 parameters of dehydroxylation of mica minerals for fault weakening, frictional heating,
648 and earthquake energetics. Earth and Planetary Science Letters, 307, 161–172.
649 Houston, J.R., Herberg, J.L., Maxwell, R.S., and Carroll, S.A. (2008) Association of dissolved
650 aluminum with silica: Connecting molecular structure to surface reactivity using NMR.
651 Geochimica et Cosmochimica Acta, 72, 3326–3337.
652 Huang, W.L., Longo, J.M., and Pevear, D.R. (1993) An experimentally derived kinetic model for
653 smectite-to-illite conversion and its use as a geothermometer. Clays and Clay Minerals,
654 41, 162-177.
655 Jackson, M.L. (1969) Soil chemical analysis – advanced course. 2nd Edition. Published by author,
656 USA.
657 Jones, B. and Renaut, R.W. (2004) Water content of opal-A: implications for the origin of
658 laminae in geyserite and sinter. Journal of Sedimentary Research, 74, 117–128.

Kaufhold, S. (2006) Comparison of methods for the determination of the layer charge density (LCD) of montmorillonites. Applied Clay Science, 34, 14–21

Kaufhold, S., Dohrmann, R., and Klinkenberg, M. (2010) Water-uptake capacity of bentonites. Clays and Clay Minerals, **58**, 37–43.

Keller, M.A., and Isaacs, C.M. (1985) An Evaluation of Temperature Scales for Silica Diagenesis in Diatomaceous Sequences Including a New Approach Based on the Miocene Monterey Formation, California. Geo-Marine Letters, 5, 31-35.

Khraisheh, M.A.M., Al-Ghouti, M.A., Allen, S.J., and Ahmad, M.N. (2005) Effect of OH and silanol groups in the removal of dyes from aqueous solution using diatomite. Water Research, 39, 922–932.

Koning, E., Gehlen, M., Flank, A.-M., Calas, G., and Epping, E. (2007) Rapid post-mortem incorporation of aluminum in diatom frustules: Evidence from chemical and structural analyses. Marine Chemistry, 106, 208–222.

Loucaides, S., Behrends, T., and Van Cappellen, P. (2010) Reactivity of biogenic silica: Surface versus bulk charge density. Geochimica et Cosmochimica Acta, 74, 517–530

LeCompte, B., Mendez, F., Jacobi, D., and Longo, J. (2008) Defining clay type using NMR and geochemical logging measurements. Society of Petrophysicists and Well Log Analysts 49thAnnual Logging Symposium, Edinburgh, Scotland, May 25-28, 2008, 1-9.

Ma, W., Song, X., Pan, Y., Cheng, Z., Xin, G., Wang, B., and Wang, X. (2012) Adsorption behavior of crystal violet onto opal-And reuse feasibility of opal-dye sludge for binding heavy metals from aqueous solutions. Chemical Engineering Journal, 193–194, 381–390.

Matheney R. K. and Knauth L. P. (1993) New isotopic temperature estimates for early silica diagenesis in bedded cherts. Geology, 21, 519–522.

682 Matteson, A, Tomanic, J. P., Herron, M. M., Allen, D. F., and Kenyon, W. E. (2000) NMR
683 Relaxation of Clay/Brine Mixtures. SPE Reservoir Evaluation & Engineering, 3, 408-413.
684 McCarty, D.K., Sakharov, B.A., and Drits, V.A. (2008) Early clay diagenesis in Gulf Coast
685 sediments: new insights from XRD profile modeling. Clays and Clay Minerals, 56, 359–
686 379
687 McCarty, D.K., Sakharov, B.A., and Drits, V.A. (2009) New insights into smectite illitization: A
688 zoned K-bentonite revisited. American Mineralogist, 94, 1653–1671.
689 Mendioroz, S., Belzunce, M.J. and Pajares, J.A. (1989) Thermogravimetric study of diatomites.
690 Journal of Thermal Analysis, 35, 2097-2104.
691 Michalopoulos, P., Aller, R.C., and Reeder, R.J. (2000) Conversion of diatoms to clays during
692 early diagenesis in tropical, continental shelf muds. Geology, 28; 1095-1098.
693 Montgomery, S.L. and Morea, M.F. (2001) Antelope shale (Monterey Formation), Buena Vista
694 Hills field: Advanced reservoir characterization to evaluate CO_2 injection for enhanced oil
695 recovery. AAPG Bulletin, 85, 561–585.
696 Omotoso, O., McCarty, D.K., Hillier, S., and Kleeberg, R. (2006). Some successful approaches to
697 quantitative mineral analysis as revealed by the 3rd Reynolds Cup contest. Clays and Clay
698 Minerals, 54, 748–760.
699 Orsini, L. and Remy J.C. (1976).Utilisation du chlorure de cobalti hexammine pour la
700 determination simultanée de la capacité d'échangeet des bases échangeables des sols.
701 Science du sol, 4, 269-275.
702 Pearson, R.T. and Derbyshire, W. (1974) NMR Studies of Water Adsorbed on a Number of Silica
703 Surfaces. Journal of Colloid and Interface Science, 46, 232-248.
704 Robertson, R.H.S. and Twedily, A.E.(1953) The biogeochemistry of Skye diatomite. Clay
705 Minerals Bulletin, 2, 7-16.

706 Rodrigues, F.A., Monteiro, P.J.M., and Sposito, G. (1999) The alkali-silica reaction. The surface
707 charge density of silica and its effect on expansive pressure. Cement and Concrete
708 Research, 29, 527–530
709 Rodrigues, F.A., Monteiro, P.J.M., and Sposito, G. (2001) The alkali–silica reaction. The effect
710 of monovalent and bivalent cations on the surface charge of opal. Cement and Concrete
711 Research, 31, 1549–1552.
712 Rondeau, B., Cenki-Tok, B., Fritsch, E., Mazzero, F., Gauthier, J.P., Bodeur, Y., Bekele, E.,
713 Gaillou, E. and Ayalew, D. (2012) Geochemical and petrological characterization of gem
714 opals from WegelTena, Wollo, Ethiopia: opal formation in an Oligocene soil.
715 Geochemistry: Exploration, Environment, Analysis, 12, 93-104.
716 Sakharov, B.A., Lindgreen, H., Salyn, A.I., and Drits, V.A. (1999) Determination of illite-
717 smectite structures using multispecimen X-ray diffraction profile fitting. Clays and Clay
718 Minerals, 47, 555–566.
719 Shukla, S.K. and Mohan, R. (2012) The Contribution of Diatoms to Worldwide Crude Oil
720 Deposits. In: The Science of Algal Fuels. (Eds.: R. Gordon and J. Seckbach), pp. 355-382.
721 Springer Dordrecht Heidelberg New York London.
722 Stoffyn, M. (1979) Biological control of dissolved aluminium in seawater: Experimental
723 Evidence. Science, 203, 651–653.
724 Strand, S., Hjuler, M. L., Torsvik, R., Pedersen, J.I., Madland, M.V. and Austad, T. (2007)
725 Wettability of chalk: impact of silica, clay content and mechanical properties. Petroleum
726 Geoscience, 13, 69-80.
727 Środoń, J. (2009) Quantification of illite and smectite and their layer charges in sandstones and
728 shales from shallow burial depth. Clay Minerals, 44, 421–434.

729 Środoń, J., Drits, V.A., McCarty, D.K., Hsieh, J.C.C., and Eberl, D.D. (2001) Quantitative XRD
730 analysis of clay-rich rocks from random preparations. Clays and Clay Minerals, 49, 514–
731 528.
732 Środoń, J. and McCarty, D.K. (2008) Surface area and layer charge of smectite from CEC and
733 EGME/H_2O-retention measurements. Clays and Clay Minerals, 56, 155-174.
734 Środoń J., Zeelmaekers E., and Derkowski A. (2009) The charge of component layers of illite-
735 smectite in bentonites and the nature of end-member illite. Clays and Clay Minerals, 57,
736 650-672.
737 Turov, V.V. and Leboda R. (1999) Application of ^1H NMR spectroscopy method for
738 determination of characteristics of thin layers of water adsorbed on the surface of
739 dispersed and porous adsorbents. Advances in Colloid and Interface Science, 79, 173-211.
740 Van Bennekom, A.J. and van der Gaast, S.J. (1976) Possible clay structures in frustules of living
741 diatoms. Geochimica et Cosmochimica Acta, 40, 1149–1152.
742 Van Cappellen, P. (1996) Reactive surface area control of the dissolution kinetics of biogenic
743 silica in deep-sea sediments. Chemical Geology, 132, 125-130.
744 Williams L.A. and Crerar, D.A. (1985) Silica diagenesis, II.General mechanisms. Journal of
745 Sedimentary Petrology, 55, 0312-0321.
746 Webb, J.A. and Finlayson, B.L. (1987) Incorporation of Al, Mg, and water in opal-A: Evidence
747 from speleothem. American Mineralogist, 72, 1204-1210.
748 Zorski, T., Ossowski, A., Środoń, J., and Kawiak, T. (2011) Evaluation of mineral composition
749 and petrophysical parameters from well logging data: the Carpathian Foredeep case study.
750 Clay Minerals, 46, 25–45.
751

Figure captions

Figure 1. Relationships between opal-A content, illite+smectite mineral group content, and the bulk rock cation exchange capacity (CEC), and mass of water desorbed at 200°C (H_2O200) in samples collected form the Monterey Fm., CA. Presented are samples rich in opal-A (opal-A zone). Linear correlation coefficient $R^2$is given for the Model I regression y=ax + b.

Figure 2. Relationships between opal-CT content, illite+smectite mineral group content, and the bulk rock cation exchange capacity (CEC), and mass of water desorbed at 200°C (H_2O200) in samples collected form the Monterey Fm., CA. Presented are samples rich in opal-CT (opal-CT zone). R^2as in Figure 2.

Figure 3. Mineral relationships between opal-A (left) and opal-CT (right) content, and illite+smectite mineral group content for samples collected in the Monterey Fm., CA, shown separately for opal-A and opal-CT zones.

Figure 4. X-ray diffraction patterns of oriented specimens of clay fractions (< 2 μm), separated from the Monterey Formation samples, Ca-exchanged and saturated with ethylene glycol (black dotted line). Mineral structures determination and quantification was performed based on the XRD pattern modeling (gray solid line).

Figure 5. Patterns of termogravimetric (TG) analysis performed on the mineral standards (left). The same analyses presented in a form of first derivative TG patterns (DTG; right).

Figure 6. Results of multiple linear correlation modeling (*Equations 1 and 2*) for CEC and H_2O200 performed separately for opal-A zone and opal-CT zones as a correlation between the measured bulk rock data (CEC_{meas}, H_2O200_{meas}) and the modeled values (CEC_{model}, H_2O200_{model}). R^2 denotes the correlation coefficient.

Figure 7. Bulk rock opal content *vs.* CEC values measured and modeled with multiple linear correlation models (*Equations 1 and 2a*). Left – unconstrained CEC_{opal} and CEC_{I+S} values;

776 middle and right – fixed value of CEC_{opal} = 20 and zero meq/100g, respectively. Fixed
777 parameters are shown in bold and underlined. Black diamonds – measured values, gray
778 circles – modeled values. Linear correlation coefficient R^2given for the Model I regression
779 between the measured and modeled CECs.
780 Figure 8.Total excess cations plotted against total excess anions for the opal-rich samples from
781 the Monterey Formation, using I-S mineral model (Table 1b) and montmorillonite model
782 (Table 1c) for excess element concentrations calculation. The black and gray trend lines
783 correspond to the respective model data points; the $R^2$is given from the Major Axis (Model II)
784 regression.
785 Figure 9. Excess (opal) CEC and excess (opal) H_2O200 values measured for opal standards
786 (Table 2) and calculated for opal contribution after subtracting the illite+smectite contribution
787 using I-S (Table 1b) and montmorillonite (Table 1c) models for the set of twelve opal-rich
788 samples from the Monterey Formation. The results of CEC_{opal} and H_2O200_{opal} modeling
789 using the full sets of the Monterey Formation samples (opal-A zone and opal-CT zone –
790 "Monterey models"), reduced for the contribution the virtual of 3% smectite, are also
791 included. The linear correlation equation is given based on the Major Axis (Model II)
792 regression for Monterey samples with both types of excess elements corrections (Table 1b
793 and c), n = 22, r^2 = 500.
794
795

Table 1. (a) Mineral and chemical composition, in wt.%, CEC, and mass loss at 200°C of selected opal-rich, clay-poor samples from the Monterey Fm., (b and c) Opal-assigned CEC and the excess element and ion concentrations calculated by subtracting contributions of individual mineral species to the total element concentrations in the bulk rock, including I-S model of the illite+smectite mineral (b), and the montmorillonite model (c).

a)

Sample	Quartz	K-feldspar	Plagioclase	Total carbonate*	Pyrite	Opal-A	Opal-CT	illite+smectite group	CEC (meq/100g)	H_2O200 (wt.%)	Total Organic C	SiO_2	Al_2O_3	Fe_2O_3	MgO	CaO	Na_2O	K_2O	TiO_2	P_2O_5	LOI
A max 1	2.0	1.0	1.0	0.0	1.0	89	1	2.0	7.3	2.4	1.55	84.81	2.08	1.14	0.24	0.35	0.98[H1]	0.32	0.096	0.1	9.56
CT max 1	3.0	0.5	1.5	0.0	0.3	0	91	3.0	11.7	3.8											
CT max 2	4.0	1.0	3.5	0.5	0.5	0	87	4.0	12.2	3.9	1.35	81.11	4.49	1.49	0.47	0.68	1.14	0.81	0.205	0.14	9.08
CT max 3	4.0	1.5	2.7	0.2	0.6	0	85	5.0	9.0	2.4	1.51	82.84	3.09	1.40	0.23	0.41	0.85	0.55	0.13	0.08	7.47
CT max 4	2.4	0.5	2.5	0.0	1.0	0	89	4.5	10.4	3.4	1.40	81.95	3.15	1.42	0.29	0.37	0.93	0.6	0.16	0.1	9.01
CT max 5	3.5	2.0	4.4	0.2	1.5	0	80	8.0	10.1	3.3		79.65	4.28	3.57	0.45	0.59	1.07[H2]	0.73	0.214	0.17	10.53
CT max 6	2.0	0.5	2.0	0.0	0.9	0	90	3.5	11.0	3.5	1.99	84.49	2.85	0.50	0.21	0.33	0.79	0.42	0.119	0.1	8.55
CT max 7	2.0	1.0	2.0	3.5	0.7	0	85	5.0	9.2	2.8	1.20	84.67	2.11	0.63	0.85	1.49	0.65	0.35	0.084	0.11	8.92
CT max 8	3.5	1.2	3.8	0.0	0.9	0	86	4.0	12.4	3.0	1.15	82.83	3.46	1.10	0.29	0.47	0.97	0.61	0.158	0.14	10
CT max 9	2.0	0.5	1.5	0.4	0.7	1	88	5.0	11.6	3.1	0.88	85.31	2.48	0.89	0.25	0.59	0.81	0.4	0.102	0.08	9.43
CT max 10	3.5	2.0	3.0	0.2	0.6	1	83	6.0	14.1		1.90	85.33	3.21	0.92	0.25	0.37	0.86	0.53	0.14	0.09	8.47
CT max 11	1.5	0.5	1.0	4.4	0.6	0	88	3.5	12.0		1.19	83.95	2.37	0.87	1.03	1.68	0.59	0.3	0.087	0.11	9.88

* Mostly excess-Ca dolomite, with traces of calcite; [H1] 0.9% of halite [H2] 0.4% of halite

803 b)
804

Sample	I-S model excess element concentration (wt.%)						I-S model excess ion (meq/100g)						Excess (opal) CEC (meq/100g)	Excess (opal) H_2O200 (wt.%)
	K	Al	Mg	Ca	Na	Fe	K^+	Na^+	Mg^{2+}	Ca^{2+}	$(AlO_2)^-$	$(Fe^{3+}O_2)^-$		
A max 1	0.06	0.58	0.11	0.22	0.28	0.31	1.6	12.0	9.4	11.0	21.6	5.6	6.8	2.53
CT max 1													10.9	3.90
CT max 2	0.41	1.29	0.16	0.30	0.53	0.76	10.5	22.9	13.4	14.8	47.8	13.6	11.3	4.14
CT max 3	0.09	0.42	0.04	0.17	0.36	0.65	2.4	15.9	3.3	8.5	15.6	11.6	7.1	2.45
CT max 4	0.29	0.65	0.11	0.19	0.44	0.48	7.5	19.4	8.8	9.7	24.0	8.7	8.6	3.49
CT max 5	0.08	0.35	0.13	0.25	0.21	1.72	2.1	9.0	10.5	12.6	13.0	30.7	6.7	3.41
CT max 6	0.17	0.70	0.07	0.18	0.39	-0.10	4.4	17.0	6.1	9.0	25.9	0.0	9.9	3.65
CT max 7	0.00	0.02	0.02	-0.01	0.27	0.03	0.0	11.8	1.5	0.0	0.7	0.5	7.2	2.86
CT max 8	0.21	0.69	0.11	0.26	0.38	0.31	5.5	16.3	9.5	12.9	25.7	5.6	11.6	3.18
CT max 9	0.11	0.31	0.03	0.14	0.43	0.24	2.8	18.7	2.3	7.2	11.6	4.3	9.7	3.03
CT max 10	-0.03	0.24	0.04	0.13	0.34	0.31	0.0	14.7	3.0	6.4	9.1	5.5	12.5	
CT max 11	0.07	0.55	0.04	0.14	0.32	0.25	1.9	14.0	3.4	7.2	20.2	4.5	11.3	

805
806

807 c)

	Montmorillonite model excess element concentration (wt.%)						Montmorillonite model excess ion (meq/100g)						Excess (opal) CEC (meq/100g)	Excess (opal) H_2O200 (wt.%)
Sample	K	Al	Mg	Ca	Na	Fe	K^+	Na^+	Mg^{2+}	Ca^{2+}	$(AlO_2)^-$	$(Fe^{3+}O_2)^-$		
A max 1	0.12	0.72	0.09	0.20	0.26	0.27	3.1	11.1	7.8	10.0	26.8	4.9	5.9	2.38
CT max 1													9.5	3.67
CT max 2	0.53	1.57	0.12	0.26	0.49	0.68	13.6	21.1	10.2	12.8	58.2	12.2	9.4	3.81
CT max 3	0.24	0.77	-0.01	0.12	0.31	0.55	6.2	13.7	0.0	6.0	28.5	9.8	4.7	2.03
CT max 4	0.43	0.96	0.06	0.15	0.40	0.39	10.9	17.4	5.1	7.5	35.7	7.1	6.6	3.14
CT max 5	0.32	0.91	0.05	0.17	0.13	1.56	8.2	5.5	3.9	8.6	33.8	27.8	2.6	2.71
CT max 6	0.28	0.94	0.04	0.15	0.36	-0.17	7.1	15.5	3.2	7.3	35.0	0.0	8.3	3.38
CT max 7	0.15	0.37	-0.03	-0.06	0.22	-0.07	3.8	9.7	0.0	0.0	13.7	0.0	4.9	2.44
CT max 8	0.33	0.97	0.07	0.22	0.34	0.23	8.6	14.6	6.2	10.9	36.1	4.2	9.8	2.85
CT max 9	0.26	0.66	-0.02	0.09	0.38	0.14	6.7	16.6	0.0	4.7	24.6	2.5	7.4	2.63
CT max 10	0.15	0.66	-0.02	0.07	0.28	0.19	3.9	12.1	0.0	3.4	24.6	3.3	9.6	
CT max 11	0.18	0.79	0.01	0.11	0.29	0.18	4.6	12.5	0.5	5.4	29.3	3.3	9.7	

808 Excess element concentrations calculated from the bulk contents corrected for the element contributions from: K-feldspar (K – 14.3%, Al – 9.7%, Na – 1%),
809 plagioclase (Ca – 1%, Na – 8%, Al – 10%), excess-Ca dolomite (Fe – 1%, Ca – 23%, Mg – 12%), pyrite (Fe – 46.5%), halite (Na – 39%); illite+smectite
810 group considered as I-S (K – 3%, Al – 16%, Mg – 1.5%; Ca – 1%, Na – 1%, Fe – 1%) or montmorillonite (Al – 9%, Mg – 2.5%; Ca – 2%, Na – 2%, Fe –
811 3%).
812 Excess (opal) CEC and excess (opal) H_2O200 calculated by subtracting the illite+smectite contribution to measured bulk rock CEC and H_2O200, using 60
813 meq/100g and 7 wt.% for I-S model and 100 meq/100 and 14 wt.% for montmorillonite model, respectively, and normalizing to the opal content.
814 Excess element concentration less than zero was approximated by zero.
815

816
817
818 Table 2.Cation exchange capacity and mass loss of mineral standards during moisture analysis tests and thermogravimetry analysis.
819

	Moisture analysis (H_2O loss at given temperature)			TG analysis (mass loss at given temperature)			
Sample	H_2O110 (%)	H_2O200 (%)	CEC (meq/100g)	H_2OTG300 (%)	H_2OTG650 (%)	H_2OTG1000 (%)	Sample origin
Opal-A 282	1.67	3.49	5.6	5.98	8.09	9.19	Santa Barbara Co., CA, USA
Opal-A 586	3.20	5.34	6.0	7.94	13.75	15.07	Auvergne, France
Opal-A 252	3.17	4.09	3.5	6.49	12.60	14.59	Monterey Formation, CA, USA
Opal-CT 417	1.48		3.6	3.63	6.34	7.11	Jalisco, Mexico
Opal-C 264	< 0.05	< 0.05	1.3	0.19	0.37	0.67	Virgin Valley, Humboldt Co., NV, USA
Tridymite 477	0.56		0.5	0.28	0.48	0.72	Germany (detailed location unknown)
Obsidian 501	0.18	0.32	0.8	0.11	0.32	0.85	Millard City, UT, USA

820
821
822

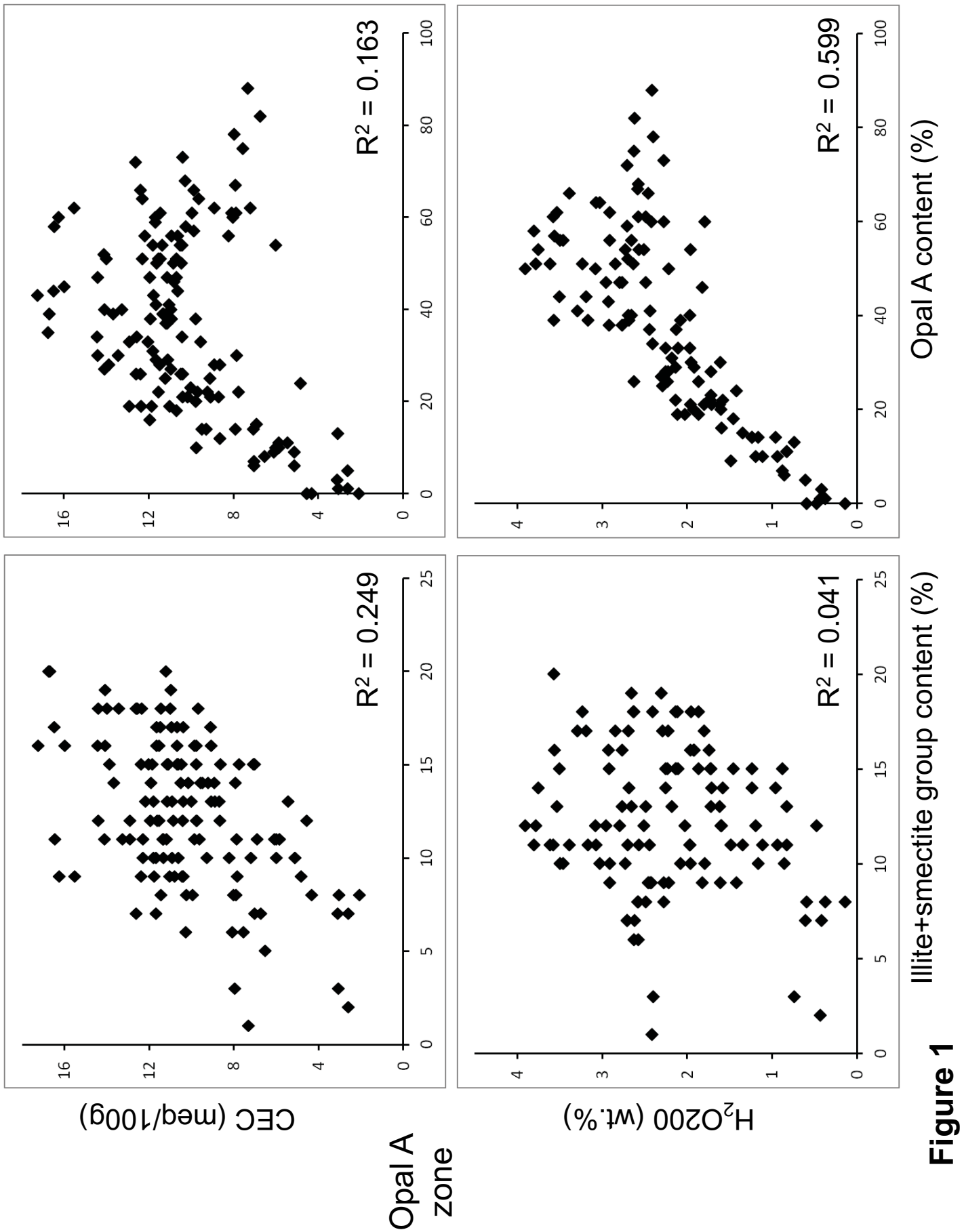
Opal A zone
CEC (meq/100g)
H2O200 (wt.%)
R2 = 0.163
R2 = 0.599
R2 = 0.249
R2 = 0.041
Illite+smectite group content (%)
Opal A content (%)

Figure 1

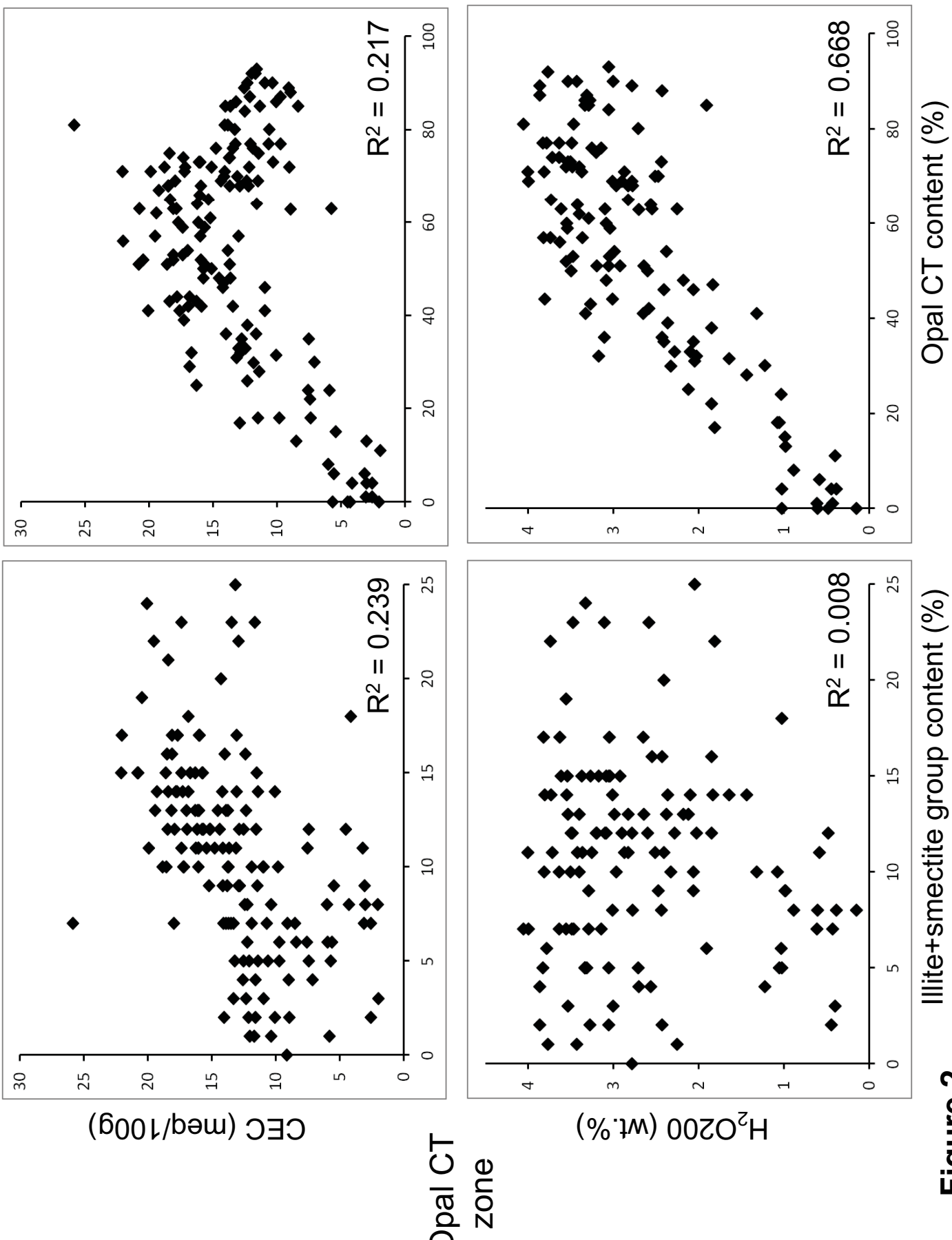
CEC (meq/100g)
H2O200 (wt.%)
Opal CT content (%)
Illite+smectite group content (%)
Opal CT zone
R2 = 0.217
R2 = 0.668
R2 = 0.239
R2 = 0.008

Figure 2

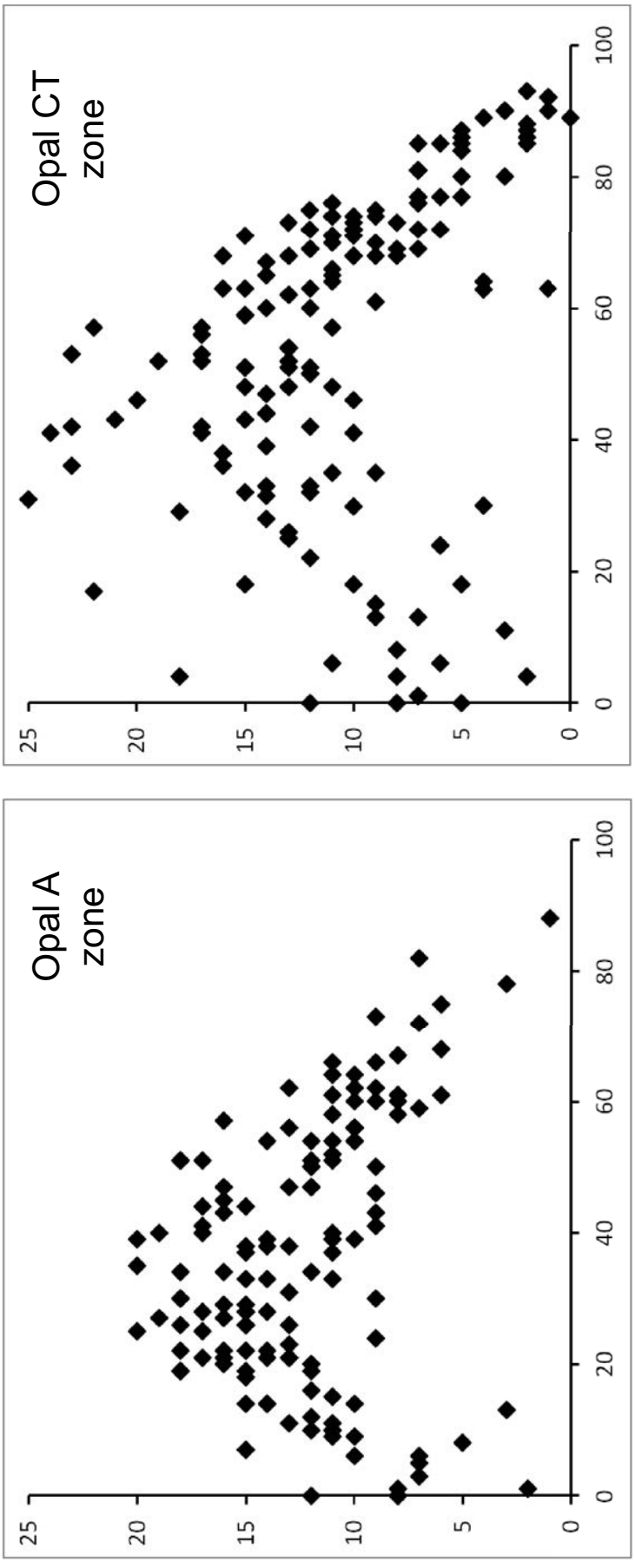
Opal A
zone
Opal CT
zone
Illite+smectite group content (%)
Opal A content (%)
Opal CT content (%)
0
5
10
15
20
25
0
20
40
60
80
100

Figure 3

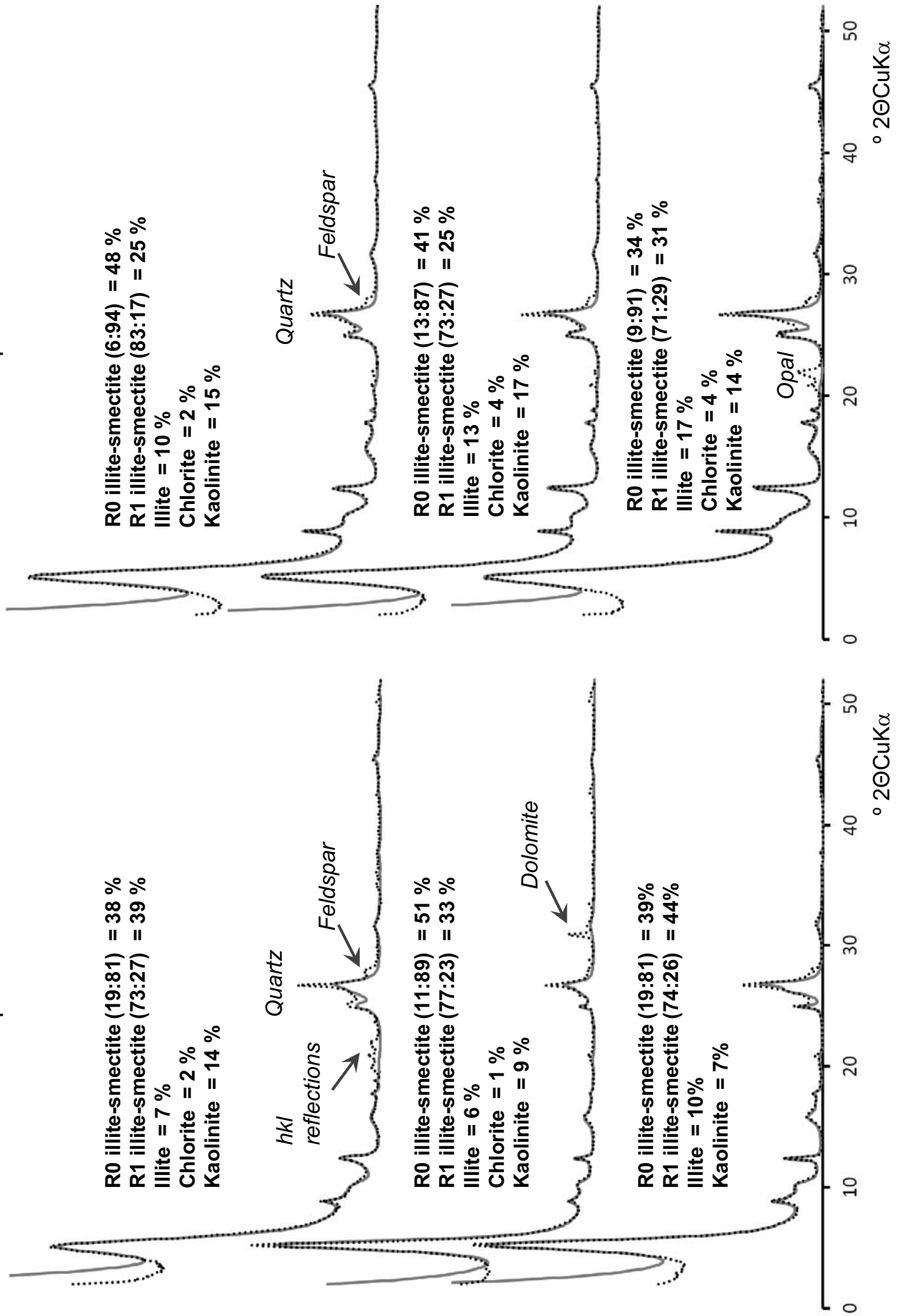
Opal A zone
R0 illite-smectite (19:81) = 38 %
R1 illite-smectite (73:27) = 39 %
Illite = 7 %
Chlorite = 2 %
Kaolinite = 14 %
hkl reflections
Quartz
Feldspar
R0 illite-smectite (11:89) = 51 %
R1 illite-smectite (77:23) = 33 %
Illite = 6 %
Chlorite = 1 %
Kaolinite = 9 %
Dolomite
R0 illite-smectite (19:81) = 39%
R1 illite-smectite (74:26) = 44%
Illite = 10%
Kaolinite = 7%
0
10
20
30
40
50
° 2ΘCuKα
Opal CT zone
R0 illite-smectite (6:94) = 48 %
R1 illite-smectite (83:17) = 25 %
Illite = 10 %
Chlorite = 2 %
Kaolinite = 15 %
Quartz
Feldspar
R0 illite-smectite (13:87) = 41 %
R1 illite-smectite (73:27) = 25 %
Illite = 13 %
Chlorite = 4 %
Kaolinite = 17 %
R0 illite-smectite (9:91) = 34 %
R1 illite-smectite (71:29) = 31 %
Illite = 17 %
Chlorite = 4 %
Kaolinite = 14 %
Opal
0
10
20
30
40
50
° 2ΘCuKα

Figure 4

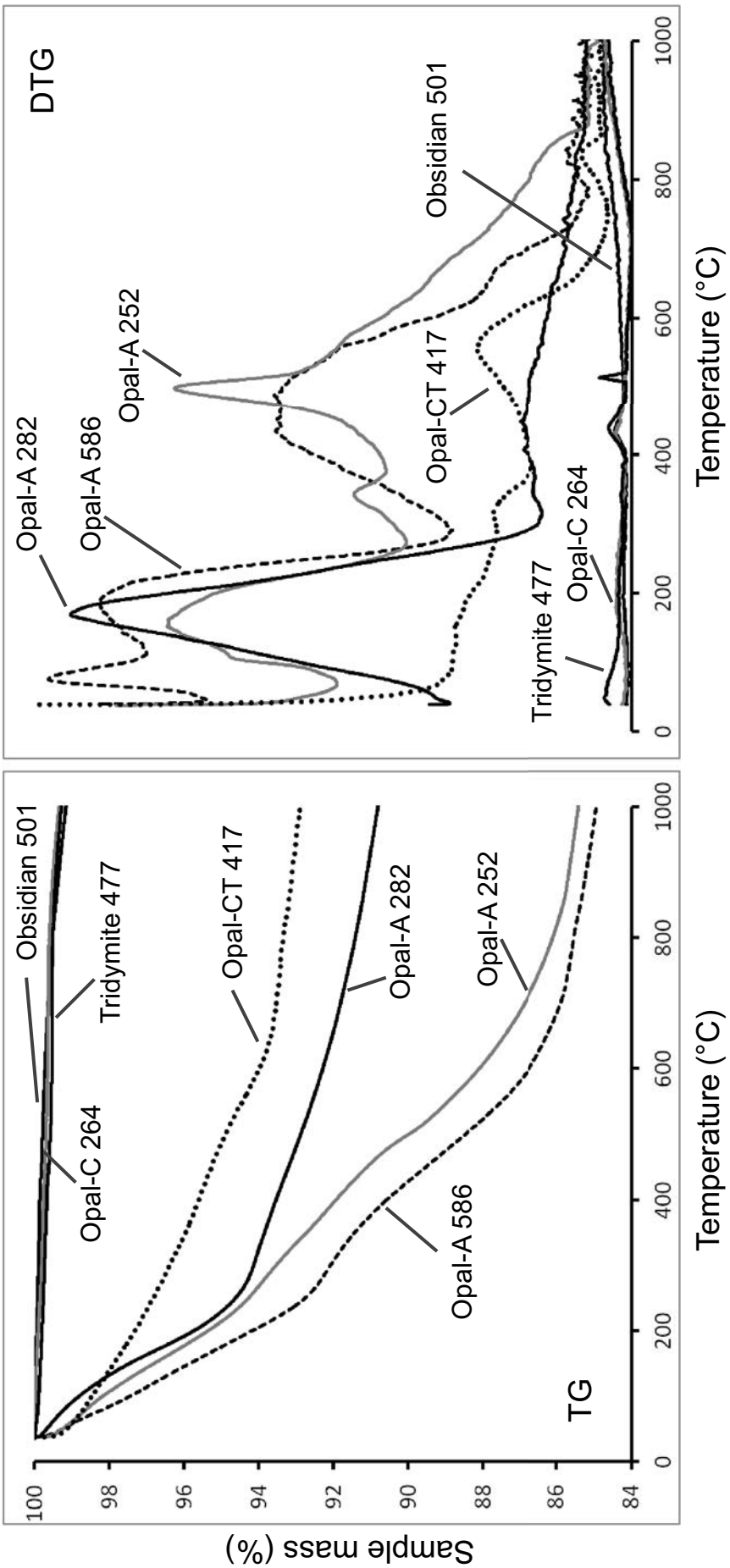
DTG
Obsidian 501
Opal-A 252
Opal-A 282
Opal-A 586
Opal-CT 417
Opal-C 264
Tridymite 477
Temperature (°C)
0
200
400
600
800
1000
TG
Obsidian 501
Tridymite 477
Opal-CT 417
Opal-A 282
Opal-A 252
Opal-C 264
Opal-A 586
Sample mass (%)
100
98
96
94
92
90
88
86
84
Temperature (°C)

Figure 5

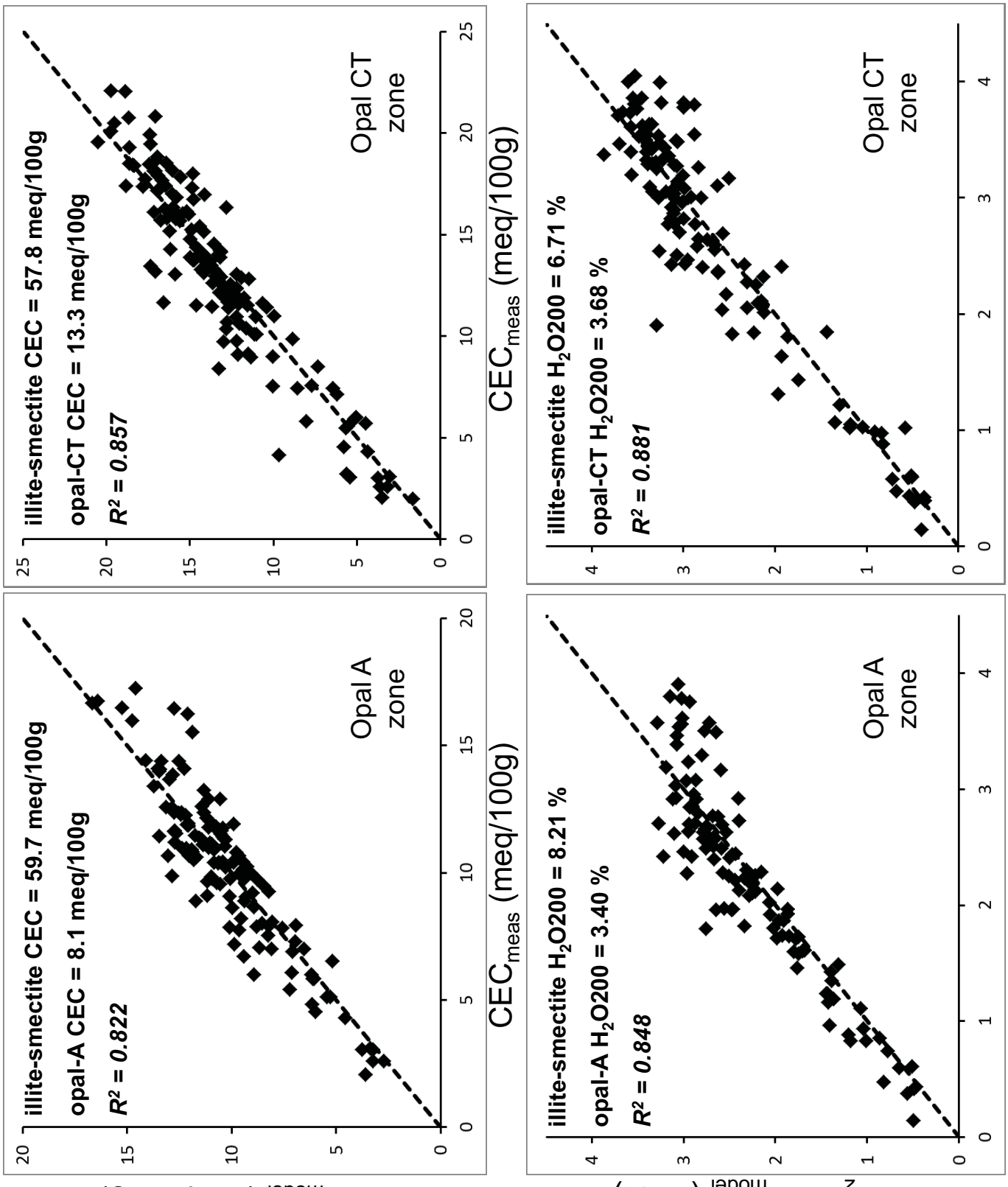
illite-smectite CEC = 59.7 meq/100g
opal-A CEC = 8.1 meq/100g
R² = 0.822
Opal A zone
illite-smectite CEC = 57.8 meq/100g
opal-CT CEC = 13.3 meq/100g
R² = 0.857
Opal CT zone
illite-smectite H2O200 = 8.21 %
opal-A H2O200 = 3.40 %
R² = 0.848
Opal A zone
illite-smectite H2O200 = 6.71 %
opal-CT H2O200 = 3.68 %
R² = 0.881
Opal CT zone
CECmodel (meq/100g)
CECmeas (meq/100g)
H2O200model (wt.%)
H2O200meas (wt.%)

Figure 6

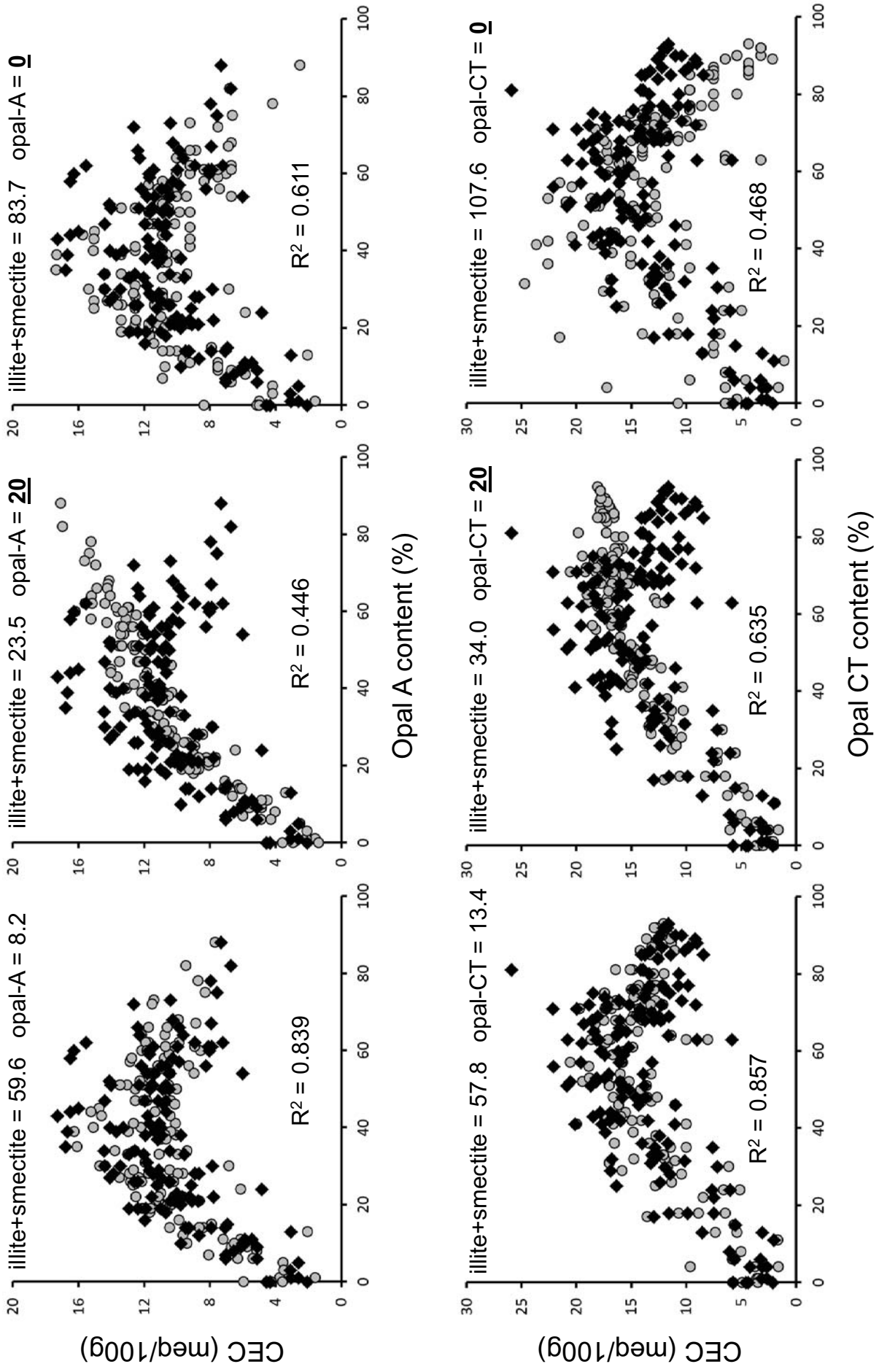
illite+smectite = 59.6 opal-A = 8.2
R2 = 0.839
illite+smectite = 23.5 opal-A = 20
R2 = 0.446
illite+smectite = 83.7 opal-A = 0
R2 = 0.611
illite+smectite = 57.8 opal-CT = 13.4
R2 = 0.857
illite+smectite = 34.0 opal-CT = 20
R2 = 0.635
illite+smectite = 107.6 opal-CT = 0
R2 = 0.468
CEC (meq/100g)
Opal A content (%)
Opal CT content (%)

Figure 7

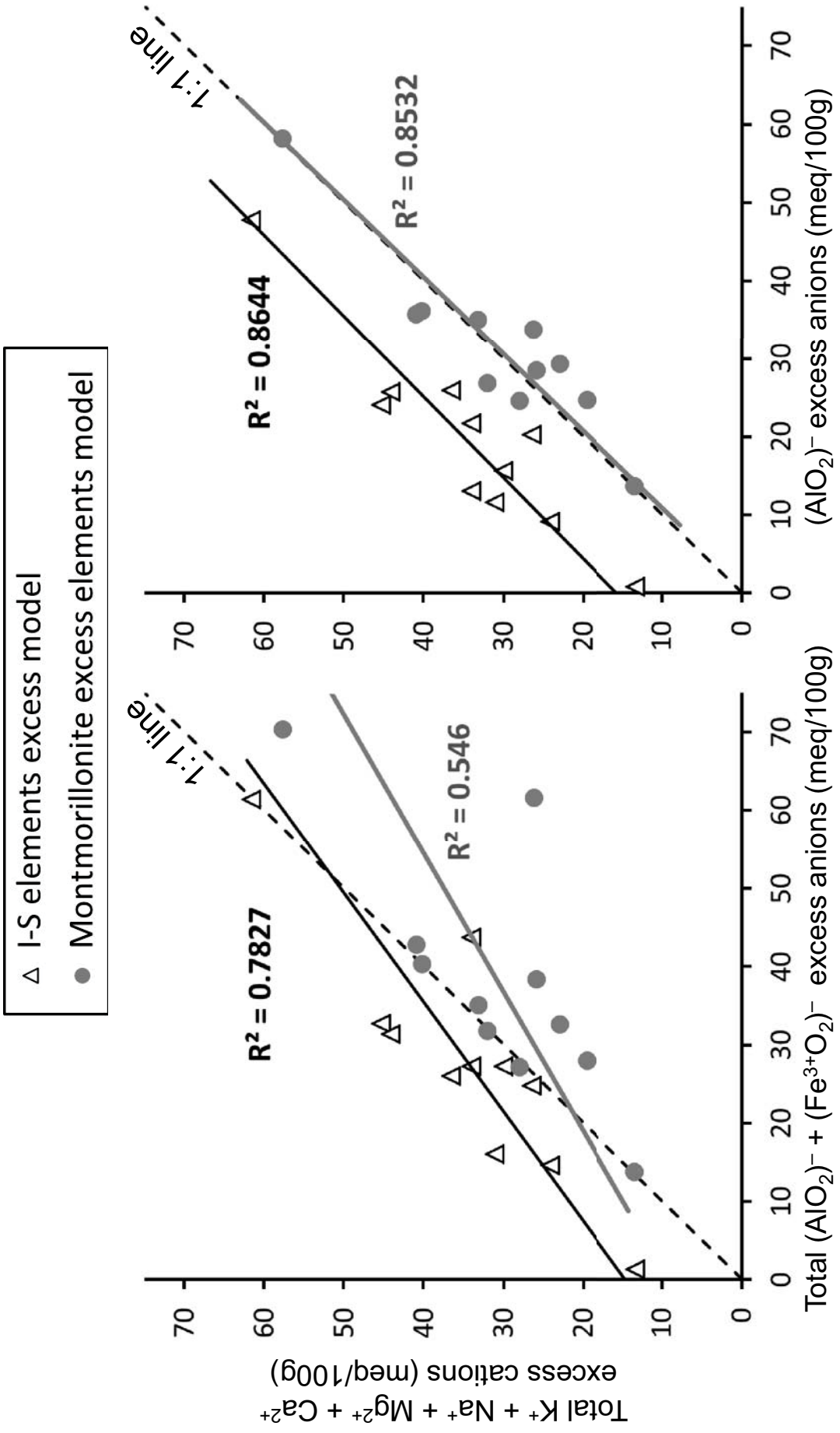
I-S elements excess model
Montmorillonite excess elements model
1:1 line
R² = 0.7827
R² = 0.546
R² = 0.8644
R² = 0.8532
Total K⁺ + Na⁺ + Mg²⁺ + Ca²⁺ excess cations (meq/100g)
Total (AlO₂)⁻ + (Fe³⁺O₂)⁻ excess anions (meq/100g)
(AlO₂)⁻ excess anions (meq/100g)
0
10
20
30
40
50
60
70

Figure 8

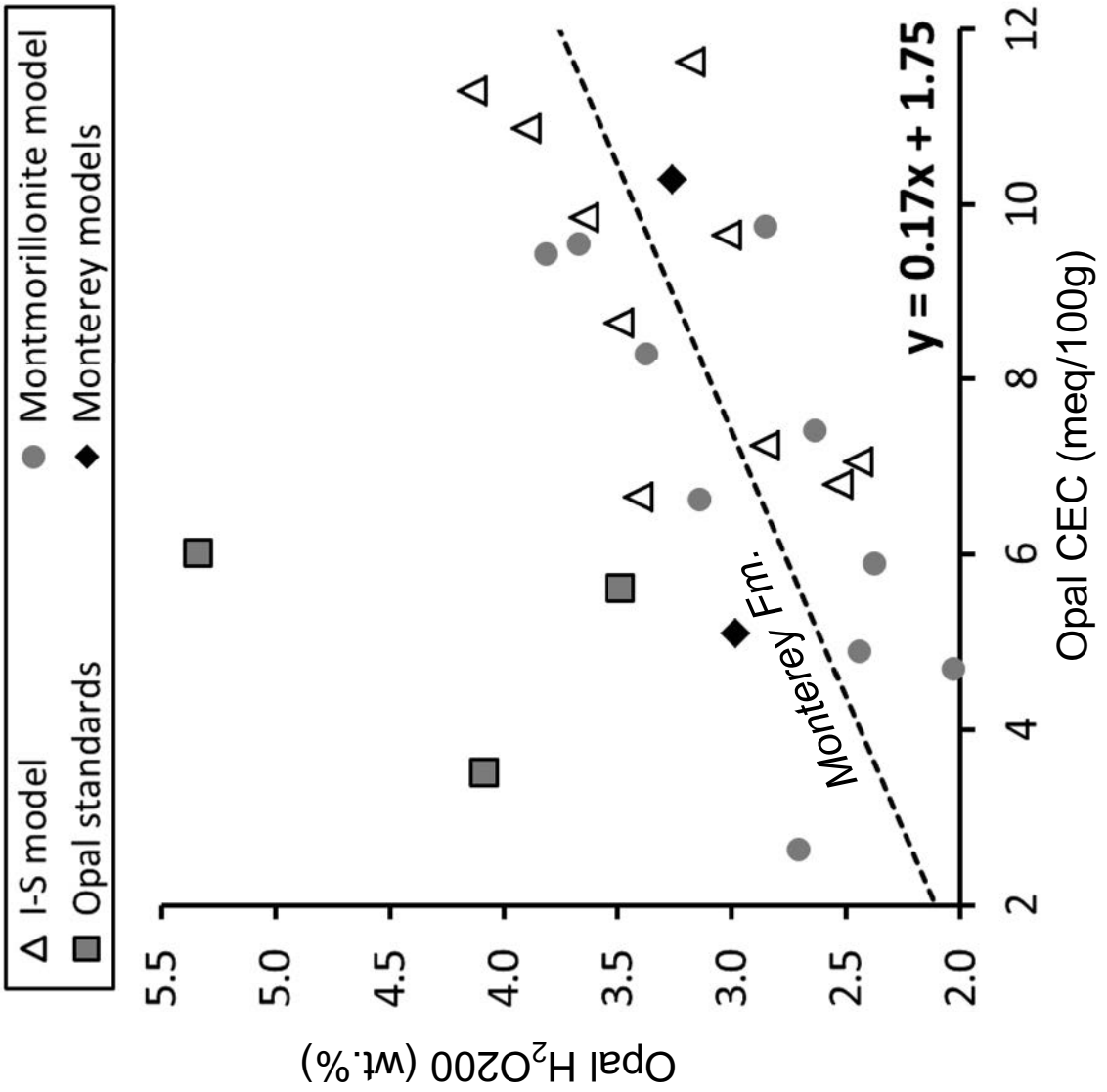
I-S model
Opal standards
Montmorillonite model
Monterey models
Opal H2O200 (wt.%)
5.5
5.0
4.5
4.0
3.5
3.0
2.5
2.0
2
4
6
8
10
12
Opal CEC (meq/100g)
y = 0.17x + 1.75
Monterey Fm.

Figure 9